DESIGN AND SIMULATION OF A FAST-CHARGING STATION FOR PLUG-IN HYBRID ELECTRIC VEHICLE (PHEV) BATTERIES

by
Makram de Freige

A thesis submitted to the Department of Electrical and Computer Engineering in partial fulfillment of the requirements of the degree of Master in Engineering

Department of Electrical and Computer Engineering,
McGill University,
Montréal, Québec, Canada
February 2011

ABSTRACT

With the increasing interest in green technologies in transportation, plug-in hybrid electric vehicles (PHEV) have proven to be the best short-term solution to minimize greenhouse gas emissions. Despite such interest, conventional vehicle drivers are still reluctant in using such a new technology, mainly because of the long duration (4-8 hours) required to charge PHEV batteries with the currently existing Level I and II chargers. For this reason, Level III fast-charging stations capable of reducing the charging duration to 10-15 minutes are being considered. The present thesis focuses on the design of a fast-charging station that uses, in addition to the electrical grid, two stationary energy storage devices: a flywheel energy storage and a supercapacitor. The power electronic converters used for the interface of the energy sources with the charging station are designed. The design also focuses on the energy management that will minimize the PHEV battery charging duration as well as the duration required to recharge the energy storage devices. For this reason, an algorithm that minimizes durations along with its mathematical formulation is proposed, and its application in fast charging environment will be illustrated by means of two scenarios.

RÉSUMÉ

Depuis le développement de l'intérêt porté aux technologies propres appliquées au domaine de l'automobile et du transport, les véhicules hybrides et électriques rechargeables (VHER) sont reconnus comme le meilleur compromis qui diminuerait les émissions de gaz a effet de serre. Malgré ce progrès pour l'environnement, la plupart des usagers de véhicules conventionnels refusent de s'adapter à cette nouvelle technologie a cause du long temps requis (4 à 8 heures) pour recharger les batteries des VHERs si les chargeurs de Niveau I et II existants sont utilisés. Pour cette raison, les stations de recharge rapide de Niveau III sont largement considérées. La présente thèse propose une station qui emploi comme sources d'énergie le réseau électrique ainsi que deux sources de stockage d'énergie : une roue d'inertie et un supercondensateur. Les convertisseurs qui permettent l'interface de ces sources avec le chargeur sont également conçus et dimensionnés en énergie. Afin d'optimiser le temps requis pour recharger la batterie du VHER ainsi que le temps requis pour recharger les sources de stockage, un algorithme est proposé avec son application à la technologie de recharge rapide. Deux différents scenarios sont mis en œuvre pour illustrer l'efficacité de cet algorithme.

ACKNOWLEDGEMENTS

I would like to thank Prof. Géza Joós, for his help, and patience during my Master degree. Through his guidance, I have drastically improved my leadership skills and gained a better idea on engineering principles and industry needs.

I would like to extend my thanks to Prof. Maxime Dubois from Laval University who leaded the project *Infrastructure for Wide Market Adoption of PHEVs* in which I was involved.

I wish to acknowledge the financial support provided by the National Science and Engineering Research Council (NSERC) and thank Auto21 Network of Centers of Excellence (NCE) that gave me many unique opportunities to practice and drastically improve my public speaking skills by delivering the results of my work in front large technical and non-technical audiences during organized contests that occurred during the following conferences and exhibitions: Canadian Manufacturers and Exporters (CME) Future of Manufacturing in Ottawa and Sustainable Manufacturing in Mississauga in February and November 2010 respectively, the Automotive Producers and Manufacturers Association (APMA) Summits in Windsor and Ottawa in June 2010 and May 2011 respectively.

Finally I would like to thank my lab colleagues: Michael Ross, Hamed Golestani Far, Aboutaleb Haddadi, Ali Jahanbani Ardakani, Samer El Itani, David Zhuang, Mike Georges, Ali Shojaei, and Moataz Ammar, who all gave me feedback on my work through my research, and helped in the beginning to get familiar with Matlab and Simulink.

TABLE OF CONTENTS

LIST OF FIGURES

LIST OF TABLES

CHAPTER 1
Introduction

This chapter gives a background of the thesis topic: Design and Simulation of a Fast Charging Station for PHEV Batteries then summarizes the work that has been conducted previously in the area of fast charging technology. The problem is then explained and the thesis outline is provided.

1.1 Background

This section defines what a PHEV is and describes briefly the equipment involved to charge it.

1.1.1 PHEV Definition

A Plug-in-Hybrid Electric Vehicle (PHEV) is a hybrid automobile with a higher-capacity battery that can be recharged by connecting the vehicle to the electrical network [1]. When the battery is below 20% capacity, a conventional combustion engine takes over and offers to the driver the same autonomy as a conventional vehicle. The PHEV has been recognized as the best short-term, economically viable opportunity for significantly reducing oil dependency and CO_2 emissions without altering motorists' driving behavior [1]. Consequently, nearly all major car makers have invested significant resources in PHEV development, and Toyota and GM delivered their first PHEVs (in small numbers) in 2010.

1.1.2 PHEV Charging Equipment

A very important impact concerns the development of the charging equipment for the market integration and daily use of PHEVs. It is essential that this equipment has the ability to:

- Quickly charge the car battery
- Modulate the electricity prices with the time of day
- Detect the state of charge (SOC) of the car battery
- Automatically bill for the electricity delivered
- Adapt to various battery types and car models

The most critical problem in charging PHEV batteries involves the car owner and public safety. Indeed the cords connecting house plugs or road stations to vehicles could cause electrical hazards. For this reason, vehicle supply equipments have been conceived in order to avoid such problems, and they consist of the three following devices [2]:

- Supply Device: Main component of the charging station, it draws power and provides shock protection.
- Power Cord: It is a cable that contains electrical current and communication signals from the charging device to the connector.
- Connector: It is simply a plug on the power cord that links the supply equipment to the PHEV charging socket.

The Society of Automotive Engineering (SAE) has been working on the J1772 standard that classifies PHEV charging stations into the five categories, listed in Table 1.1 below [2, 3].

Table 1.1. PHEV Charging Modes Characteristics [2, 3]

Type	*Location*	*Power Level (kW)*	*Charging Duration*
Level 1: 120 VAC	On-board	1.2 – 2.0	18 hours
Level 2 (low): 208 – 240 VAC	On-board	2.8 – 3.8	8 hours
Level 2 (high): 208 – 240 VAC	On-board	6 – 15	4 hours
Level 3: 208 – 240 VAC	Off-board	> 15 - 96	20 – 50 min
Level 3: DC Charging: 600 VDC	Off-board	> 15 - 240	20 – 50 min

1.1.3 History of Fast Charging

The importance of a network of charging stations is already established as a critical part of the PHEV and electric vehicle (EV) technologies. In the future, charging stations may play the same role as gasoline stations today. In Israel (2011), Denmark (2011), Australia (2012) and Portugal, governments have already set targets in place for a large penetration of charging stations in the urban environment [4], [5]. US Company Better Place is a leader in this field and plans to install hundreds of thousands of Level I and Level II AC charging stations in these countries. General Motors plans to release the Chevy Volt EV in 2011, with a battery capacity of 16 kWh and a Level I, on-board charger of power 3.3 kW [6].

There is currently a lack of fast-charging units. As an alternative, urban facilities have been proposed where the discharged car batteries would be swapped with charged battery packs.

However, at the recently held Alternative Fuels and Vehicles conference, a panel of representatives from some American electric car makers suggested that they would prefer fast charging stations to the battery swapping scenario. The impact of fast charging on battery degradation is a critical parameter that needs to be taken into account [7].

1.2 Literature Review

The current section summarizes previous works that have been conducted concerning the charging and fast charging stations, and all areas that are closely related to them.

1.2.1 The Level III Charger

Among the three classes of charging stations, the Level III is the most interesting and practical one for installations in public places like commercial areas since it enables an easier integration of PHEVs and EVs into the market. For this reason, many developed countries are planning on using Level III, off-board quick chargers, especially in Western Europe [8]. In Japan, the Tokyo Electrical Power Company has announced the installation of 200 10-minute high power chargers for 2010, which will coincide with the introduction of the Mitsubishi i-Miev EV, which is already advertized with a quick-charge DC plug [9]. This is the result of a structural characteristic of Tokyo, where drivers do not have access to a plug at their homes to charge their cars.

1.2.2 Existing PHEVs

Some American companies have already built prototypes of such fast charging stations: a prototype that boasts an expected 10 min charge time has been launched during the third quarter of 2010 [10], and the LSV-100 Zip prototype that can charge in less than 30 min [11]. In Europe in January 2010, Renault-Nissan announced its success in the development of a fast-charging station that is capable of replenishing 80% of an EV car battery in less than 30 min [12].

1.2.3 Fast Charging Outcomes

Besides charging a battery car to 80% of its SOC in typically 15 minutes [13], fast charging also decreases operating costs and increases productivity in two ways [14]:

- Fast chargers are known to be more efficient than conventional chargers, and charging with less overcharging increases the battery efficiency.
- Fast charging technology increases the vehicle speed.

The main issues in fast charging reside in the four main failure mechanisms of industrial lead acid batteries [14]:

- Positive Active Material (PAM) Shedding
- Corrosion of the positive plate grid
- Imbalance among battery cells
- Suffocation of negative plate

1.2.4 Conventional Charging Schemes

In a bidirectional battery charger, charging can be accomplished in two ways [15]:

In constant current/constant voltage mode, the battery is first charged in constant current mode to 70% SOC then it is charged in constant voltage mode.

In order to implement fast charging, several algorithms and methods have been found, and among them is a fully digitized smart method involving a combination of high continuous constant charging current and some charging pulse current. Such techniques consider the actual charge state of the battery and the battery previous charges and discharges [16]. However, the method that has revealed as being the most practical one and as having the best efficiency and the shortest charging time is the pulse-charged method. It basically consists of creating a large-time charging pulse that is immediately followed by a very short-time discharging pulse, followed then by a “waiting period” [16].

1.2.5 Power Electronics Systems

The Level III fast charging station provides DC power via a DC connector [17] by drawing power from AC or DC sources. The conversion from AC to DC (or vice-versa) and among them is done through the converters mentioned in Table 1.2 below [18, 19].

Table 1.2. Main Power Electronics Converters [19]

Conversion	AC to AC	DC to DC	AC to DC	DC to AC
Topology	AC Controller	Chopper	Rectifier	Inverter

Power electronics can be found in many applications such as reactive power compensation, long distance transmission lines, and power transfer from one side to a higher voltage side [18]. The basic configuration of a Level III charger consists of cascading a voltage source converter (VSC) with a chopper; a configuration similar to an HVDC system [20]. Indeed once the power is drawn from the grid, its AC form will be converted to DC form via the VSC (and vice-versa) [21]. The chopper will allow the change in the charger terminal voltage in order to adapt to various output voltages depending on the car battery. Such converters are also used when connecting any storage device to the charger DC link [22]. For example a flywheel requires an AC/DC, whereas supercapacitors require choppers. These last are mainly demanded for electrical energy storage in batteries and for uninterruptible power supplies (UPS) [23]. The major topologies that have been found so far are:

- Converters employing two voltage-type bridge converters; used for “interfacing an energy storage device in an autonomous power system [23]”.
- Interleaved multichannel converters; which have been designed primarily in order to optimize the converter efficiency by varying the number of active channels [24, 25].
- Variable duty cycle converters; which suits the most for a battery charger. The output voltage of the DC/DC converter is perpetually imposed by the battery voltage, whereas the input converter voltage must remain the same. It is thus sure that the converter duty cycle (being the ratio of these two voltages) must be variable. A method for the switching of such converters has been proposed: it is based on shifted PWM signals with a variable duty cycle [26].

1.2.6 Thermal Management in Battery Fast-Charging

When being quickly charged, vehicle batteries are subject to temperature elevation because of the resistive (Ohmic) losses and the electrochemical reactions that occur during both the battery charging and discharging processes [27].

The use of Thermoelectric Generators (TEG) has been proposed in order to accelerate the cooling process in batteries in order to increase the battery life and use it in the automotive sector. Such coolers can be placed either between the two terminals of a cell pair or a plate pair [27]. An algorithm has been proposed for power-flow management where all the energy storage devices must be charged up to their respective specified SOC before the whole system runs [28]. Also a hybrid PWM method has been proposed in order to reduce the temperature rise in converters, without increasing considerably the switching losses. In such methods half of the total number of switches is switched at high frequency (in the order of tens of kHz) whereas the other half is switched at the system frequency (50 or 60 Hz). Such methods have proven to be very successful [29].

1.2.7 Additional Charger Applications

A bidirectional charger is also capable of achieving two supplementary functions: vehicle to gird (V2G) and vehicle to home (V2H); both of which are main topics of research in the PHEV's integration within the power grid. V2G corresponds to connecting the PHEV to the grid and then using the power of the car battery in order to meet the grid demand [30], while V2H corresponds to connecting the PHEV to the home electrical circuit in order to meet the home electrical demand [30]. While the V2G impact on the grid stability will be seen in the next section, the V2H impact will not be studied in this thesis.

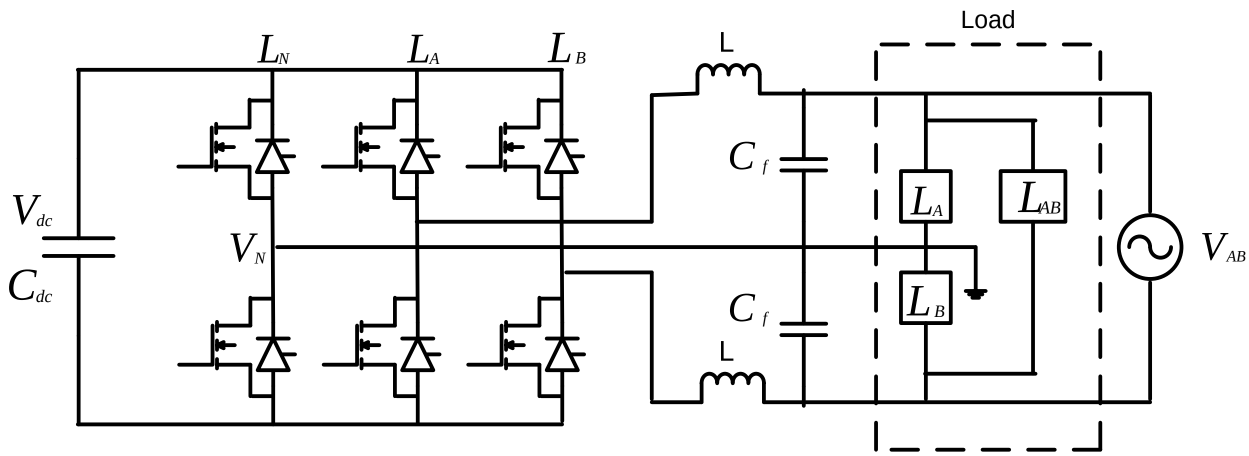

Figure 1.1. Grid-side Converter [Based on 30]

Control schemes have been implemented for the grid-side converter of a single AC source charger modeled in Figure 1.1, in three modes of operations: Charging mode, V2G mode, and V2H mode [30].

In the structure of Figure 1.2, showing a control scheme for V2G mode, $G_c(s)$ is the compensator and $G_f(s)$ is the feed-forward loop compensator [30]. Unlike the MPPT function in wind applications or PV, which tries to draw the maximum power from the sources, V2G function considers the battery pack health. For this reason, the reference current magnitude i_L* is generated by the grid real power command instead of the DC voltage loop [30]. The phase information is obtained via a PLL.

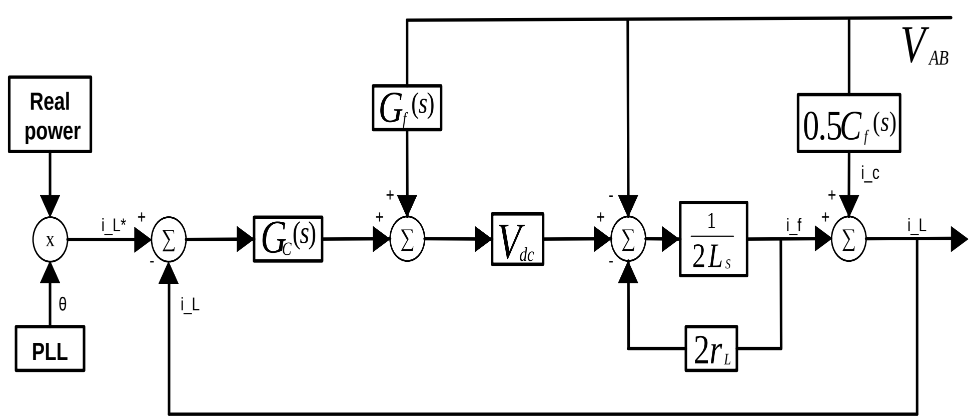

Figure 1.2. Control Scheme for V2G Mode [Based on 30]

The structure of Figure 1.3 that displays a control scheme for the charging mode is designed with an inner current loop and an outer voltage loop [30]. Also a PI controller is added in order to generate with the phase (via the PLL) the reference current magnitude [30].

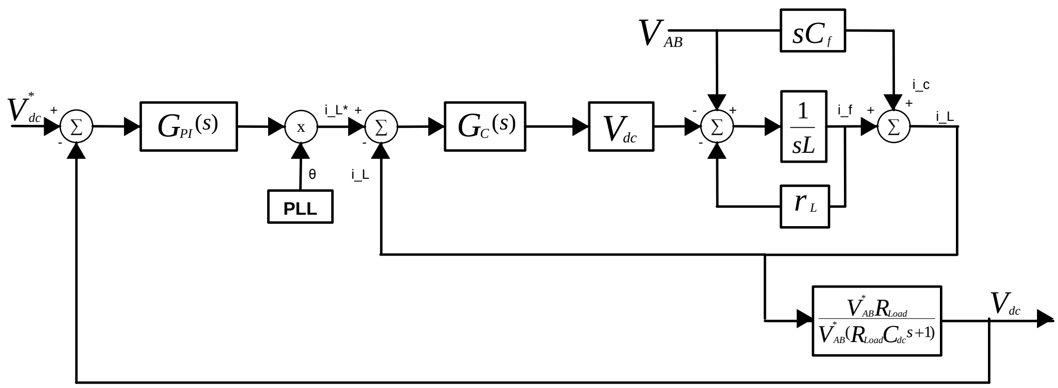

Figure 1.3. Control Scheme for Charging Mode [Based on 30]

In the two previous modes of operation, two major kinds of harmonic pollution appeared [31]: The first one is caused from the fact that the phase voltage reference was taken directly from the grid voltage, which caused the apparition of harmonics arising from the grid due to the phase reference of the input current. Thus, the harmonic pollution played a role in the reference in the current loop, which is undesirable [31]. The second one is the 2nd order harmonic on the DC bus voltage. For this reason the control methods of [30] have been improved by adding to the previous structures an internal voltage reference and a 2nd order notch filter in order to attenuate such sources of pollution [31].

1.2.8 Impacts of PHEV Deployment on the Grid

The current section summarizes the challenges faced with PHEV penetration to the grid as well as the offered ancillary services.

1.2.8.1 Challenges

When PHEVs are not connected to the grid during off-peak load periods they may have significant effects on the power system network. Indeed a new peak demand period will be faced causing utilities to get stressed [32, 33]. Furthermore there will be excessive reactive power injections [34, 35] and harmonics causing troubles such as burning capacitors or reactors located at some substations [32]. Current harmonics injection will also have a bad impact on the power quality of distribution systems [36]. A new infrastructure including transformers and power distribution lines will thus be necessary [37].

The previous problems have been analyzed by considering a group of 10 households where half of the PHEVs are being charged from the utility, and each one draws a power of 2 kW [37]. The results were that not only the demand in power would increase by 20 kW, but also such additional loads exhibit nonlinear current characteristics due to the presence of harmonics. This is shown in Figure 1.4.

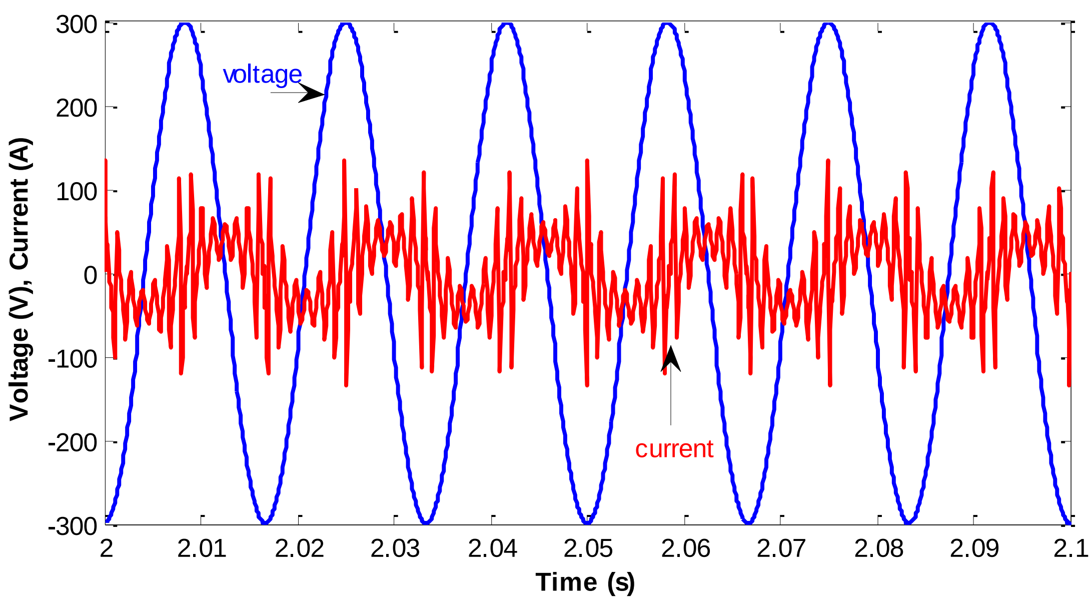

Figure 1.4. Nonlinear Load Characteristics [Based on 37]

Studies have been conducted to estimate the THD of such currents, and they confirm that through the years new technologies have been developed to reduce the current THD. It has been shown that the current THD has been largely improved from typically 20% in 1993 to typically 3.72% in 1995 [34]. The study demonstrated also that when a large number of chargers operate at the same time, there will be harmonics cancellation, and thus the cumulative current THD and power factor will also be improved [35]. The majority of the current harmonics are odd because due to the symmetry on positive and negative half-cycles, the even harmonics have negligible amplitudes [36]. A typical load current spectrum is displayed in Figure 1.5 below.

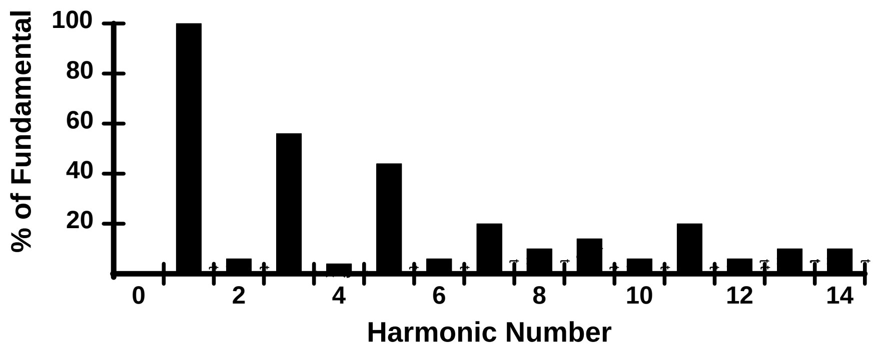

Figure 1.5. Typical Load Current Spectrum [Based on 34]

Power system stability will also be affected due to the large amount of reactive power drawn from the grid; it is defined as the ability of a system to be back in its equilibrium state of operation following a disturbance [37]. Load characteristics and active power demand are also factors that influence voltage stability. The critical parameters affecting voltage stability are found as follows:

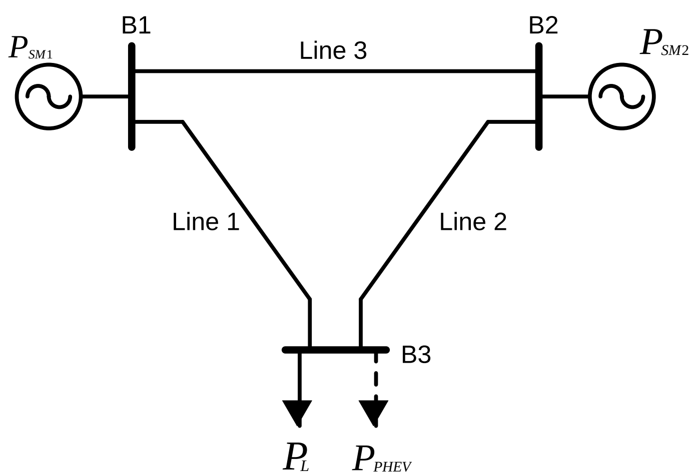

Figure 1.6. Three-bus Power System
for Voltage Stability Analysis [Based on 37]

In Figure 1.6 above, the active and reactive power flow between buses 1 and 3; denoted P_{B13} and Q_{B13} are calculated as:

$$P_{B13} = \frac{V_1 \cdot V_3}{X} \cdot \cos(\delta) \tag{1.1}$$

$$Q_{B13} = \frac{V_1^2 - V_1 \cdot V_3 \cdot \cos(\delta)}{X} \tag{1.2}$$

Newton-Raphson power flow analysis is now used to compute the Jacobian matrix, whose singular solutions constitute the critical values to be found [37]:

$$\begin{bmatrix} \Delta P_{B13} \\ \Delta Q_{B13} \end{bmatrix} = \begin{bmatrix} \frac{\partial f_1}{\partial \delta} & \frac{\partial f_1}{\partial V_3} \\ \frac{\partial f_2}{\partial \delta} & \frac{\partial f_2}{\partial V_3} \end{bmatrix} \cdot \begin{bmatrix} \Delta \delta \\ \Delta V \end{bmatrix}$$

The previous procedure gives that $V_1 = 2 \cdot V_3 \cdot \cos(\delta)$. Furthermore, the relationship between the load active and reactive power, P_L and Q_L, and the load angle, φ, is the following:
$Q_L = P_L.\tan(\varphi)$. By combining the last result with the expressions for P_{B13} and Q_{B13}, we get:

$$\tan(2\delta) = \frac{-1}{\tan(\varphi)}$$

Consequently, the following critical values for voltage stability are obtained for $P_{L\text{-critical}}$, $Q_{L\text{-critical}}$, and $\delta_{critical}$ [37]:

$$\delta_{critical} = \frac{1}{2} \tan^{-1}\left(\frac{-1}{\tan(\varphi)}\right) \tag{1.3}$$

$$P_{L\text{-critical}} = \frac{V_1^2 \cdot \tan(\delta_{critical})}{2X} \tag{1.4}$$

$$Q_{L\text{-critical}} = \frac{V_1^2 \cdot \tan(\delta_{critical})}{2X} \cdot \tan(\varphi) \tag{1.5}$$

1.2.8.2 Ancillary Services

Besides the challenges encountered previously, additional services are provided by the electric utility under a regulated market; referred to as ancillary services [38]. These include the following:

- Voltage support: The fact that the charging stations' power electronic converters can consume and supply reactive power can be used for voltage support applications.

- Load tracking and frequency regulation: The bidirectional power transfer of PHEV battery chargers allows stationary PHEVs to be used as generators.
- Peak shaving: When PHEVs produce electricity the stored battery energy could be used for peak shaving, which results in an important decrease of line current and losses, and thus reducing transmission upgrade costs.
- Network stability services: Other PHEV functions include power system stabilizers and backup generators in case of a contingency. This last feature improves the system reliability.
- Backup energy source: When being parked, PHEVs act as energy storage devices [39], and thus can supply energy in exchange for monetary profits [40]. Energy storage is also very useful to allow the operation of microgrid islanding [39].

1.2.8.3 Integration Studies

Many Canadian utilities (like Hydro-Quebec, BC Hydro, Manitoba Hydro, and Hydro One Networks) are concerned with the impact of PHEV integration on electric distribution systems and the creation of implementation standards [41, 42, 43].

Particularly, Hydro-Quebec is involved in a study with EPRI on the impacts on the distribution grid of a wide deployment of PHEVs including: Transformer and transmission line thermal loading, voltage regulation and harmonics, and transformer loss of life. The study assumes: various PHEV charge profiles and penetration across utility customers, different charge times and battery state of charges [41]. The followed methodology displayed in Figure 1.7 consisted of a deterministic and a stochastic analysis [44].

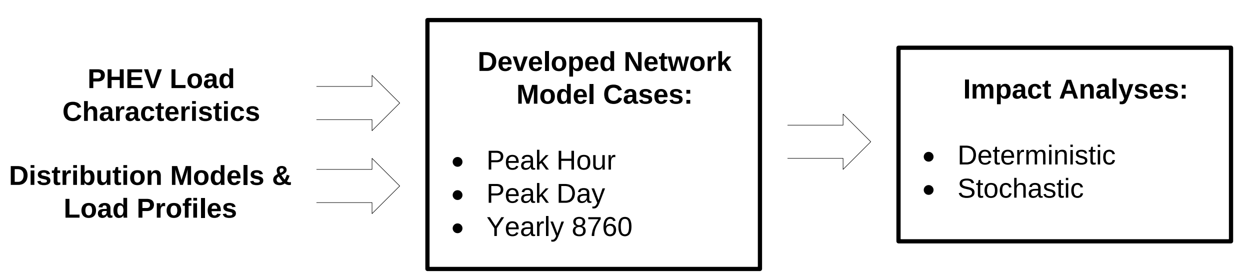

Figure 1.7. System Impact Analysis Framework [Based on 44]

The deterministic analysis is developed to identify the impact on the system distribution components and the general trend in network behavior for forced scenario without considering the spatial and temporal diversity of PHEV loads on the grid [44]. On the other hand, the stochastic analysis shown in Figure 1.8 takes into consideration the previous factors and the obtained results enable an understanding of which impacts are the most probable to occur [44].

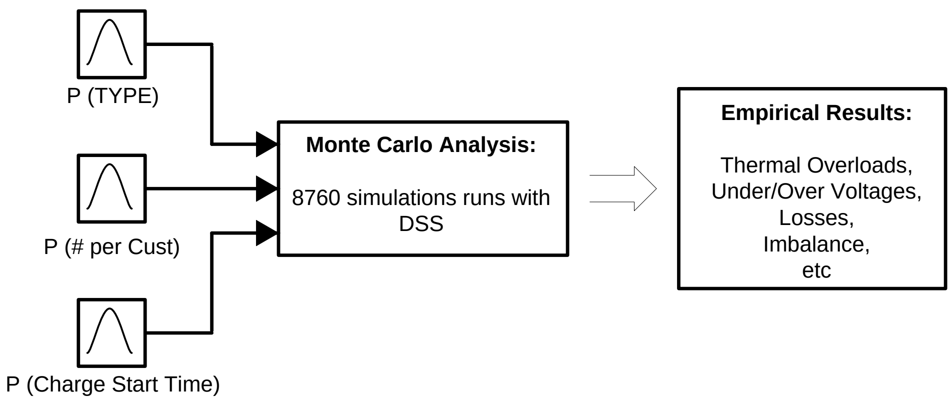

Figure 1.8. The Stochastic Approach [Based on 44]

While the stochastic analysis is still in progress, the deterministic one revealed that:

The average transformer lifespan is very sensitive to an increase in PHEV loading. The transformer aging and peak hot spot temperatures are displayed in Figures 1.9A and 1.9B, respectively, for various charging profiles [44]:

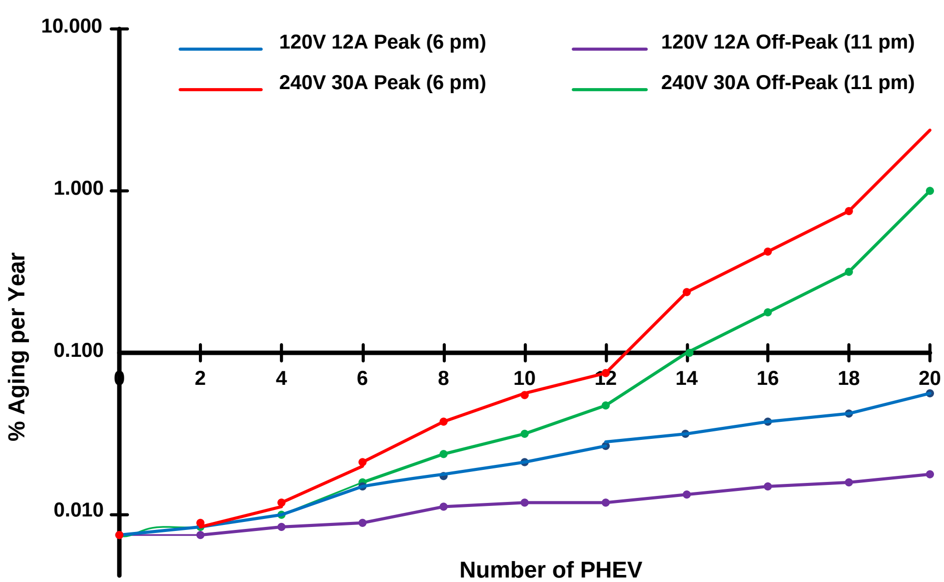

Figure 1.9A. Transformer Yearly Aging [Based on 44]

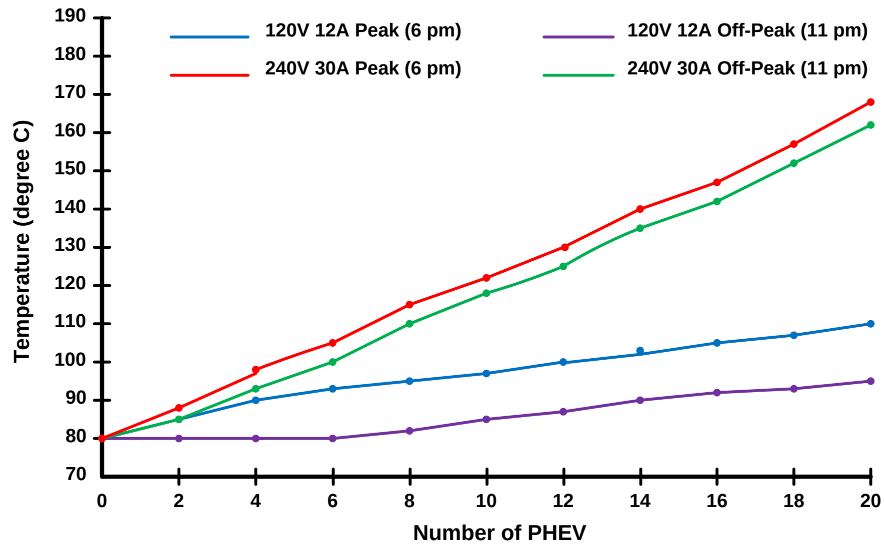

Figure 1.9B. Transformer Hot Spot Temperatures [Based on 44]

The charge profile is the main factor that influences the number of overloaded elements, which increases with increasing PHEV penetration, as shown in Figure 1.10 [44]:

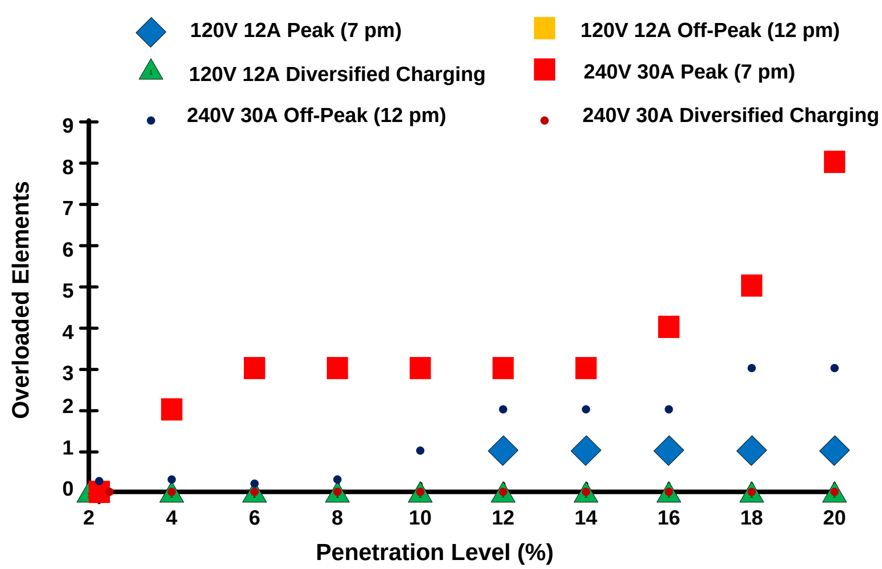

Figure 1.10. Number of Transformers for which Normal Rating Is Exceeded for Deterministic PEV Penetration [44]

1.2.9 PHEV Batteries

A device that converts chemical to electrical energy (and vice versa) is called a battery [45]. The parameters listed in Table 1.3 below can be seen on any battery data sheet that is provided by the battery manufacturer.

Table 1.3. Battery Technical Specifications [45]

Parameter	***Unit***	***Parameter***	***Unit***	***Parameter***	***Unit***
Nominal Voltage	V	Power Density	W/L	Internal Resistance	Ω
Cut-off Voltage	V	Maximum Continuous Discharge Current	A	Specific Power	W/kg
Capacity	A.h	Maximum 30-sec Discharge Pulse Current	A	Energy Density	W.h/L
Energy	W.h	Charge Voltage	V	Specific Energy	W.h/kg
Cycle Life	(unitless)	Float Voltage	V	Charge Current	A

Among these parameters, the main ones that will be useful to conduct the present research are briefly explained below [45]:

- Nominal voltage: It is also referred to as the reference battery voltage.
- Cut-off voltage: It is the voltage at which the battery is considered “empty”.
- Charging voltage: It is the maximum allowed voltage when charging the battery.
- Nominal energy: It is the available Watt-hours of the battery (Power (W) multiplied by time (h)).
- Charging current: It is the ideal value of the current at which the battery is charged in the beginning (at constant current) to approximately 70% state-of-charge (SOC).

The main chemistries of PHEV batteries are: Lead-acid, lithium-ion (Li-ion), and NiMH [46]. Lead-acid batteries have revealed as being the most popular ones due to the following advantages that they have that distinguish them from their counterparts [47]:

- They are the best option to be used in fast charging technology.
- Fast charging prolongs their life cycle.
- The pulsed-type algorithm that will be used later in this thesis has the beneficial property of keeping the best oxide morphology over life cycle.

The main factors that influence the battery life cycles are the battery temperature and DOD (Depth of Discharge) [48]. Figure 1.11 below shows that batteries with lower DODs and temperatures possess a higher number of life cycles.

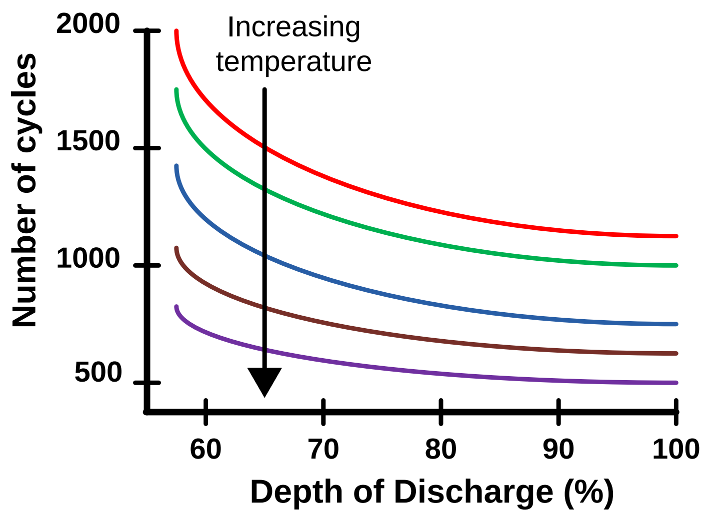

Figure 1.11. Impact of DOD and Temperature on Battery Cycles [48]

1.2.10 Stationary Storage Devices

Devices capable of accumulating some energy for a finite duration before restoring it to the circuit are referred to as energy storage devices. Many kinds of stationary storage devices can be used in order to accumulate some energy: superconducting coils, flywheels, supercapacitors, and hybrid energy devices.

1.2.10.1 Storage Coils

Also known as superconducting magnetic energy storage (SMES) [49], such devices are known to have the highest energy density. The following mathematical relation relates the coil energy stored E (in J) to the coil inductance L (in H) and the current that traverses it (in A) [50]:

$$E = \frac{1}{2} \cdot L \cdot I^2 \tag{1.6}$$

Storage coils found their use in many sectors:

- The space sector where they are designed for satellites as solenoids due to their simple construction and preferred structural mass over other types of magnets [51].
- The transportation sector where coils are mainly used in high-speed rail locomotive leading to higher fuel efficiency, lower prime mover weight and power rating, and especially faster locomotive thus leading to a shorter trip time [52]. Coils are also applied in automatic guided vehicle to allow contact-free energy transmission [53] by transferring energy using the magnetic energy stored in the coil.
- The stability sector where they are used to improve the transient stability of a system if they are controlled appropriately; for example using a fuzzy-logic control scheme [54].

The main drawbacks of SMES are the measures of protection that need to be taken in order to reduce the conduction losses; for example, the design and implementation of generic commutation circuits for the charging and discharging processes [55].

1.2.10.2 Flywheels

Flywheel energy storage (FES) is an electromechanical device that stores energy in kinetic form in a rotating mass [49]. Flywheels are useful when there exist an imbalance between the generated power and the powere demanded by the load [56]. In such devices, the charging and discharging processes are done by varying the rotational velocity of the mass: to store some electricity, a motor converts the external electrical energy into mechanical energy (charging), on the other hand to deliver some energy the motor acts as a generator and converts the energy into electrical form (discharging) [56]. Some control strategies have been found in order to apply flywheels in EVs. One of them has been found in [57], where the charging process is done through the use of fuzzy logic and a PI controller whereas the discharging is done by simply applying the PWM strategy to the interfacing converter (AC/DC) [57].

The energy E (in J) that can be stored in a flywheel rotor can be found using the wheel moment of inertia J (in $Kg.m^2$) and angular speed ω (in rad/s), in the following mathematical relation [58]:

$$E = \frac{1}{2} \cdot J \cdot \omega^2 \tag{1.7}$$

FESs have been recognized as being the cleanest energy storage devices [59] and find their applications in the following areas:

- Previously, FESs have always been used for short-term energy storage in rotating machines and engines to deliver smooth power [58].
- Recently, they are being used for electrical energy storage [60]. In such case the FES is referred to as a mechanical battery energy storage device: it always stores kinetic energy, and releases it in electrical form upon demand. This last advantage will be considered largely in this thesis.
- For the next few years, researches are being conducted in order to design higher specific power density (kW/Kg) and higher specific energy (kWh/Kg) density. The first one depends completely on the motor/generator that drives it [60].

Any FES is composed of four major parts: a rotor, a rotor bearing, a container, and a power interface [59]. Figure 1.12 below displays the main flywheel parts.

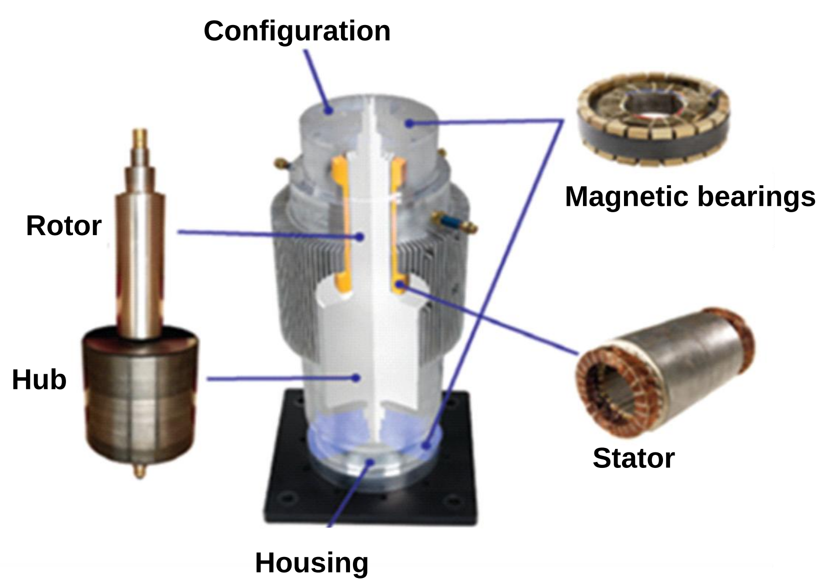

Figure 1.12. Main FES Components [59]

The steady-state energy losses in flywheels are mainly due to the drag forced that is induced by the magnetic field of the superconductor magnetic bearing and permanent magnet (PM)-type motor/generator (PMSM/G) [61]. However, the largest losses occur from the PMSM/G, and an acceptable solution would be to simultaneously rotate the PMSM/G and the PM [62].

1.2.10.3 Supercapacitors

Also known as electric double layer capacitors (EDLC) or ultracapacitors, such devices behave exactly like any normal capacitor with the differences of having a much higher capacitance (in the order ranging from tens to hundreds of Farads) and a higher power density which lets them charge and discharge rapidly [63], and allows them to be used in applications to replace batteries. A typical supercapacitor is shown in Figure 1.13 below.

Figure 1.13. A Typical Supercapacitor [63]

Such devices store energy using the following mathematical relation that relates the energy stored E (in J) to the capacitance C (in F) and the voltage across it U (in V) [50]:

$$E = \frac{1}{2} \cdot C \cdot U^2 \quad (1.8)$$

They are classified into three categories [64]:

- Double-layer capacitors depend on the double electric layer mechanism.
- Electrochemical capacitors rely on the fast Faraday oxydo-reduction reactions.
- Hybrid capacitors are a combination of the two previous categories.

A control strategy has been proposed for the supercapacitors to support current peaks that are momentarily demanded by electrical road vehicles. Such a method is based on the fact that the supercapacitors must be discharged once the current demanded by the load becomes greater than the reference limit current for battery discharge [65].

Supercapacitors are safe, possess an average light weight, can be recycled, and are environmentally friendly [66], which is what makes them mostly popular in the domain of energy storage for traction applications [67] and elevator systems with a soft commutated interface [64]. Additional applications include the following:

- Diesel-electric locomotives power assistance: supecapacitors are preferred compared to electromechanical accumulators when being used in power assistance [68].
- Recuperation of the braking energy that is wasted in the braking resistors [69].
- Sole energy storage device in hybrid electric cars if they are dimensioned appropriately.

Despite the benefits just mentioned, the energy that can be stored in a supercapacitor is low, which prevents large vehicle autonomy. For this reason, some methods have been found in order to allow fast energy transfer between supercapacitors in transport applications, such as the introduction of sequential supply [70].

1.2.10.4 Hybrid Energy Storage Systems

The energy storage devices described above can be combined together to form a new energy storage system. In the case where two of them are combined together, the resulting system is referred to as hybrid energy storage.

A hybrid system based on compressed air and supercapacitors has been designed to meet its maximum efficiency at any time. All the system devices are reversible, meaning they can charge and discharge [71]:

- During generation, the compressed air is liberated in the pneumatic machine that operates as a motor to power the DC generator.

- During storage, the machine acts as a motor that drives the pneumatic machine that operates as a compressor to fill the tank with air under pressure.

Such a system has been proved as being too sensitive regarding multiple conversions, and the efficiency of each of the system components has been found to be low [72]. This mean that such equipment must be designed very carefully to ensure that it is practical [72].

1.3 Problem Statement

Fast charging of PHEV batteries means that the duration required to charge such batteries must be minimized, which implies the use of the grid and additional sources of energy that must be managed efficiently and intelligently.

A waiting period is also required to recharge the storage devices once the PHEV leaves the station. Such a period should also be minimized in order to reduce the time that the client needs to wait at the station before charging the battery, and to accelerate the battery swapping process at some charging stations if applicable.

Finally, it is important to look at some aspects of the impacts caused by such charging stations on the grid such as harmonics, THD, phase unbalance, power factor, ground fault and electricity generation.

1.4 Contributions

The present research proposes the design and presents the simulation results of a fast-charging station capable of recharging PHEV batteries with capacities lower or equal to 15 kWh from a minimum of 20% to a maximum of 95% of the battery state-of-charge in a maximum duration of 15 minutes. After a battery has been charged, a waiting period (during which no cars have access to the charging station) of a maximum duration of 7.5 minutes is required. During this period, the storage devices are being recharged to their maximum.

The charging station employs the grid and two stationary storage devices; both with high power densities, environmentally friendly, with a high efficiency, and that are capable of charging and discharging in durations in the order of minutes. An algorithm that manages the three energy sources in order to reduce the charging and waiting durations has been developed.

While the charging station may introduce harmonics on the grid, it does not affect the power factor, and is more efficient than a conventional charger.

1.5 Thesis Outline

The present thesis follows an outline described below:

Chapter 2 describes the basic configuration used for the design of the fast charging station: energy requirements and storage devices choice.

In Chapter 3, the different power electronic interfaces (including choppers and rectifiers/inverters) of the charging station are designed.

Chapter 4 presents the individual control schemes of each converter as well as the control and proposed algorithm of the whole charging station.

In Chapter 5, the charging station operation is simulated with two different scenarios: the first one displays the charging process of a single PHEV battery whereas the second one displays the charging process of two consecutive PHEV batteries.

Chapter 6 summarizes the performance of the proposed solution and proposes future work to be improved in the fast charging station design.

CHAPTER 2
Charging Station Basic Configuration

This chapter justifies the necessity of storage technology in addition to the electrical grid in the fast charging station design, then quantifies the grid and local storage need, and finally justifies the use of a flywheel and a supercapacitor as the station storage devices.

2.1 Grid Power Limitation

The long duration required to charge PHEV batteries (4 to 8 hours) with the currently existing Level I and II chargers is due to the fact that such chargers use the grid only as an energy source to charge the PHEV battery [73]:

Typical PHEV and EV parameters are displayed in Table 2.1 below [74, 75].

Table 2.1. Nominal Voltage and Energy for PHEV/EV Batteries

	Nominal Voltage (V)	*Nominal Energy (kWh)*
PHEV	180 – 270	10 – 15
EV	Above 300	20 – 60

Assuming a power factor, pf, the maximum duration, Δt_{max}, required to charge a PHEV battery from the grid from 20% to 95% of its maximum capacity E_{max} = 15 kWh is found as:

$$\Delta t_{max} = \frac{E_{max} \cdot (SOC_{max} - SOC_{min})}{P_{grid}} = \frac{E_{max} \cdot (SOC_{max} - SOC_{min})}{V_{RMS} \cdot I_{RMS} \cdot pf}$$

Table 2.2 below displays the maximum PHEV battery charging durations in Europe and North America; given their respective grid voltage and current [76].

Table 2.2. Maximum PHEV Battery Charging Duration

	RMS Voltage (V)	*RMS Current (A)*	*Power Factor (pf)*	*SOC_{min} (%)*	*SOC_{max} (%)*	*E_{max} (kWh)*	*Δt_{max} (hours)*
Europe	230	16	0.95	20	95	15	3.2
North America	120	15	0.95	20	95	15	6.6

Table 2.2 illustrated the insufficiency of the grid to charge a PHEV battery in less than an hour. For this reason, additional energy sources are necessary to reduce the battery charging time. As an example, the grid current of 20 A was insufficient, so the McGill Racing Team uses as an additional source its dynamometer - used for testing batteries and electric motors - that can also provide power. A motor is mounted on the dynamometer as a generator to charge the batteries at much higher rates, raising the current to about 90 A. The team hybrid car uses a battery whose specifications are: a capacity of 45 A.h at 0.2 C, and a continuous charging current of 180 A in order to be fully recharged in 15 minutes (fast-charging) [77].

Another way to minimize the maximum charging duration is to use the energy storage technology [78]; where the energy is being stored in storage devices before being delivered to the load. This method will also enable a minimum reliance on the electrical grid in order to diminish the impact on the grid of the additional load. More on this topic will be discussed in Chapter 6.

2.2 Station Energy Sources Quantification

The designed fast charging station uses, in addition to the grid, the energy storage technology. The law that relates the charger output energy E_O (kWh) to the grid energy E_{Grid} (kWh) and the energy storage devices energy $E_{Storage}$ (kWh) is the following:

$$E_O = E_{Grid} + E_{Storage} \tag{2.1}$$

The grid is interfaced with the charger via an AC/DC converter.

According to the SAE J1772, the Level 3 fast-charging station employs DC charging with 600 V, as mentioned in Table 1.1 [3]. For this reason, the design will assume a voltage V_{DC} = 600 V on the DC side. The design will also assume on the DC side a grid current $I_{Grid,DC}$ = 50 A in order for the charging station to draw a maximum power of 30 kW from the grid.

The charging station is also designed to charge a typical PHEV battery in a maximum duration of Δt_{max} = 15 minutes. The grid helps the battery charging process during a maximum duration of Δt_{Grid} = 10 minutes (shown in Chapter 5). The grid energy is calculated as follows:

$$E_{Grid} = V_{DC} \cdot I_{DC} \cdot \Delta t_{grid} = 600 \text{ x } 50 \text{ x } \frac{1}{6} \Leftrightarrow E_{Grid} = 5 \text{ kWh} \quad (2.2)$$

As mentioned in Section 1.4, the charging station is designed to charge PHEV batteries whose energy capacities do not exceed 15 kWh, from a minimum of 20% of the battery state of charge (SOC) to a maximum of 95% of the battery SOC. This implies that the maximum energy output by the charger will be:

$$E_{O,max} = E_{PHEVmax} \cdot (SOC_{max} - SOC_{min}) = 15 \cdot (0.95\text{-}0.20)$$

$$\Leftrightarrow E_{O,max} = 11.25 \text{ kWh} \quad (2.3)$$

Using (2.1), (2.2), and (2.3), the maximum energy provided by the charging station storage devices, $E_{Storage,max}$, can be found as follow:

$$E_{Storage,max} = E_{O,max} - E_{Grid} = 11.25 - 5$$

$$\Leftrightarrow E_{Storage,max} = 6.25 \text{ kWh} \quad (2.4)$$

The energy management in the designed charging station is summarized in Table 2.3 below.

Table 2.3. PHEV Charging Station Energy Management

Sources	***Grid***	***Storage Devices***	***Output***
Energy (kWh)	5	6.25	11.25

The choice of the charger storage devices is developed in the next section.

2.3 Station Storage Devices Choice

The present section lists the most popular stationary energy storage devices performance requirements, and then justifies the charging station devices choice.

2.3.1 Performance Requirements

The chosen energy storage devices must ideally satisfy all of the following performance criteria in order to maximize the fast charging station efficiency:

- Dynamicity: The charging station is designed to charge a battery in a maximum 15 minutes (short duration). The storage device must thus be able to charge and discharge in this period.
- High Power Density: The device must be able to deliver a high amount of power in a short period of time.
- High Efficiency: The charging station must meet its maximum possible efficiency. This last criterion depends on the main station parts: converters, storage devices, etc. Therefore, it is a must to consider the storage devices that have the highest efficiency.
- Environmentally Friendly: The device must have no or negligible negative impacts on the environment.

Table 2.4 below displays the most popular stationary storage devices according to the previously mentioned criteria [71, 72].

Table 2.4. Classification by Criterion

Storage Technology	***Life time (cycles)***	***Power Density***	***Efficiency (%)***	***Impact on the Environment***
Flow Batteries	1500 – 2500	Low	75 – 85	Medium
Metal-Air Batteries	100 – 200	Low	50	Medium
NAS Batteries	2000 – 3000	Low	89	High
Lead-Acid Batteries	200 – 300	Medium	75	High
Li-Ion Batteries	300 – 500	Medium	95	Medium
Supercapacitors	10000 – 100000	High	93 – 98	Low
Flywheels (FES)	$10^5 – 10^7$	High	90	Low

2.3.2 Storage Devices Choice

As seen in Table 2.4 batteries have significant impacts on the environment, possess medium efficiencies, and relatively low power density and number of life cycles. Thus, they do not satisfy any of the performance requirements.

On the other hand, the FES and the supercapacitors have both: low impacts on the environment, high efficiencies, power densities, and life cycles. Additionally they can both be charged and discharged in a duration in the order of minutes [58]. The only drawback they both present is their low energy density [79], which is not considered an issue since we are seeking high power density instead.

However, the use of only one of them is not appropriate for the following reasons:

Even being a power device, the supercapacitor can provide a high amount of power for a duration that is smaller than the PHEV battery charging time (15 minutes) [58]. Furthermore a large capacitance would be required, which increases the supercapacitor cost.

The time required to charge an FES is relatively long (10 minutes), which will significantly increase the time that a PHEV user will have to wait at the charging station before the PHEV battery is reasonably charged.

A way to overcome the above problems is to combine a flywheel and a supercapacitor as a system representing the fast charging station energy storage device in addition to the electrical grid, as shown in Figure 2.1 below. The suitable performance of such a combination will be seen in Chapter 5.

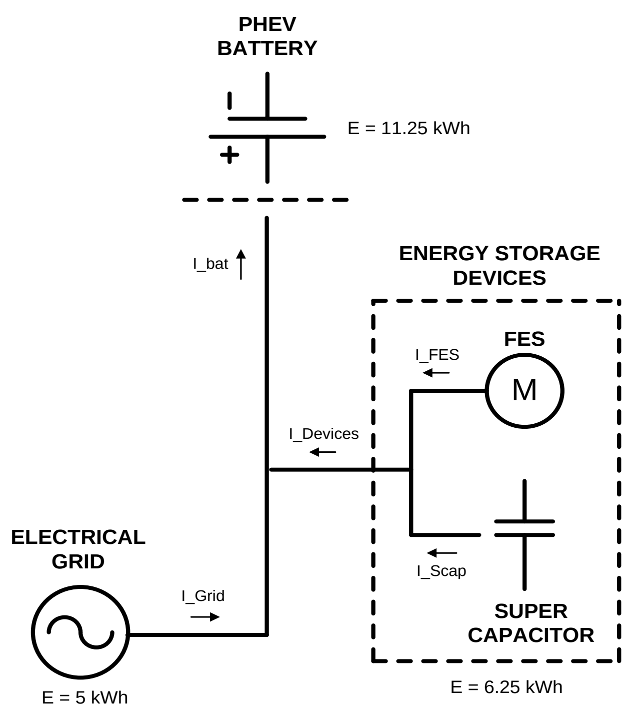

Figure 2.1. Charging Station Basic Design

CHAPTER 3
Power Electronic Interfaces

The designed fast charging station is composed of three energy sources: the grid, an FES, and a supercapacitor. The last two sources are interfaced with the charger DC link via power electronic converters [58, 64]. Also, since the car battery voltage is variable from one car battery to another, a DC/DC converter must be placed on the charger output in order to adapt the charger output voltage to the battery voltage. The present chapter discusses the individual design of such converters, and then gives the electrical specifications of the whole charging station.

3.1 Static Power Switches

This section covers the existing technologies of static power electronic switches and then justifies the use of IGBT as the best option for the design of the converters.

3.1.1 Existing Technologies

The most popular controllable static switches used in the design of the power electronic converters of Table 1.1 are displayed below in Table 3.1 [19].

Table 3.1. Main Controllable Switches Comparison

Device	***Power Capability***	***Switching Speed***
MOSFET	Low	Fast
IGCT	High	Slow
IGBT	Medium	Medium

3.1.2 Chosen Technology

In order to allow bidirectional power transfer, the switches used in the converter legs must conduct the current in both directions. The switches must also be completely controllable. For this reason, the use of diode and thyristor is eliminated since the former is completely uncontrollable and the latter is semi-controllable.

Furthermore, the grid outputs a real power of 30 kW (see Section 2.2), and has a frequency of 60 Hz; both are in the medium range of operation. In the technologies of Table 3.1, the IGBT tends to be the best option for the design of the charging station is power electronic interfaces. An IGBT converter has an efficiency of typically 90% [58].

3.2 Grid Side Converter

The grid provides single-phase AC voltage and current. In order to be interfaced with the charger's dc bus, a bidirectional AC/DC converter is required in order to allow the station to operate in V2G mode as well [30].

3.2.1 Converter Design

In order to turn on and off the controllable switches inverters and rectifiers, many types of gating signals can be used, among them are [19]:

- Square wave inverters: DC input has to be varied to control the magnitude of the output AC voltage.
- Voltage cancellation: Switches operate at 0.5 duty cycle while the DC input remains fixed.
- Pulse-Width-Modulation (PWM): A modulating signal where the AC side frequency is compared with a carrier having a frequency such that the frequency modulation m_f (defined below) is a large odd integer:

$$m_f = \frac{f_{carrier}}{f_{control}}$$

The most popular gating generation used in inverters is a sinusoidal PWM, where the control signal is a sine wave; it generates harmonic voltages in the range of the switching frequency and higher, which can be easily filtered out [19]. The grid-side converter is shown in Figure 3.1.

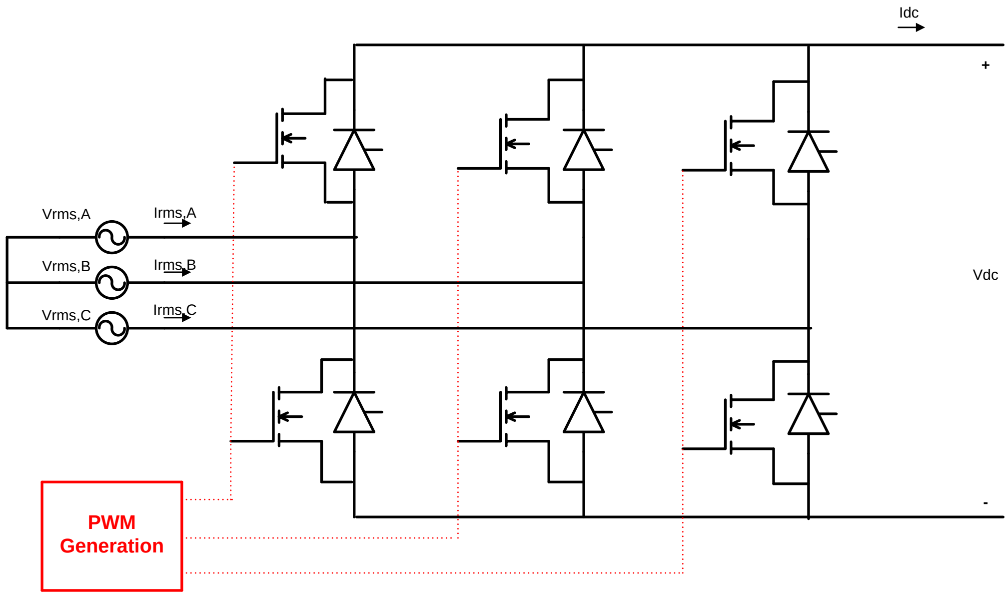

Figure 3.1. Grid-side Converter

3.2.2 Electrical Specifications

The converter is designed with IGBT switches, so its efficiency ή is typically 0.9 (see Section 3.1.2), and it is designed with an output DC power of 30 kW (see Section 2.2).

$$ή = \frac{P_{DC}}{P_{AC}} = 0.9 \Leftrightarrow P_{AC} = \frac{P_{DC}}{0.9} = \frac{30}{0.9} = 33.3 \text{ kW} \quad (3.1)$$

The restriction imposed on the voltage on the DC side is the converter switches loss of control limit [80]. Indeed, the IGBT anti-parallel diodes must be kept reversed-biased in order to not conduct in the wrong direction during the charging mode of operation (power transfer from AC to DC side). This can be achieved if the output DC voltage is kept above the line-to-line grid peak voltage value. The design also assumes a DC bus voltage of 600 V (see Section 2.2) so that the previous restriction translates to:

$$V_{DC} > \sqrt{2}.V_{Grid,ll,RMS} = \sqrt{2}..\sqrt{3}.V_{Grid,RMS} \Leftrightarrow V_{Grid,RMS} < \frac{600}{\sqrt{6}} \Leftrightarrow V_{Grid,RMS} < 245 \quad (3.2)$$

Following condition (3.2), the SAE J1772 Standard in Table 1.1, and the fact that the grid voltage varies typically between 0.95 and 1.05 pu [37], choosing the grid voltage on the AC side to be 220 V is an acceptable option to remain within the constraint imposed by (3.2). Assuming a power factor of typically 0.95 and with equation (3.1), the grid current can be found as follows:

$$P_{AC} = 3.V_{Grid,RMS}.I_{Grid,RMS}.pf$$
$$\Leftrightarrow I_{Grid,RMS} = \frac{P_{AC}}{3.pf\ .V_{Grid,RMS}} = \frac{33\ 333}{3.(0.95)(220)} \Leftrightarrow I_{Grid,RMS} = 53\ \text{A} \quad (3.3)$$

With section 2.2 and the results found in (3.1) – (3.3), the following Table 3.2 can be drawn.

Table 3.2. Grid Converter Electrical Specifications

	Input Side (RMS Values)	***Output Side (DC Values)***
Grid Voltage (V)	220	600
Grid Current (A)	53	50
Real Power (kW)	33.3	30

3.3 Flywheel Energy Storage (FES) Converter

When acting as a generator, an FES converts kinetic energy into electrical energy [58]. This can be translated in the following way: when rotating at an angular speed ω (rad/s), the energy is converted into AC currents that must be converted to DC currents via an AC/DC converter [81].

3.3.1 Converter Design

The FES converter must also be bidirectional in order to allow both charge and discharge of the FES.The converter may be single-stage (flywheel ISG a.c. ⇔ d.c. bus), or double stage (flywheel ISG a.c. ⇔ d.c. bus ⇔ a.c. network) [58]. In this case, the simple single-stage case is needed since the interface is to be done with the charging station dc bus. The FES converter looks exactly like the grid-side converter that has been shown in Figure 3.1 previously.

3.3.2 Electrical Specifications

The FES is designed to provide a maximum output power of 30.75 kW (see Chapter 5). With a DC bus voltage of 600 V, the output current on the DC side is:

$$I_{DC} = \frac{P_{DC}}{V_{DC}} = \frac{30\ 750}{600} \Leftrightarrow I_{DC} = 51.25\ \text{A} \quad (3.4)$$

When the FES is discharged, it charges back form the electrical grid. Furthermore since it is interfaced with the DC bus via an IGBT converter, the input AC power must be:

$$ή = \frac{P_{DC}}{P_{AC}} = 0.9 \Leftrightarrow P_{AC} = \frac{P_{DC}}{0.9} = \frac{30.75}{0.9} = 34.17 \text{ kW} \quad (3.5)$$

With the same grid voltage and power factor, the grid current can be found as follows:

$$P_{AC} = 3 \cdot V_{Grid,RMS} \cdot I_{Grid,RMS} \cdot pf$$

$$\Leftrightarrow I_{Grid,RMS} = \frac{P_{AC}}{3 \cdot pf \cdot V_{Grid,RMS}} = \frac{34\,170}{3.(0.95)(220)} \Leftrightarrow I_{Grid,RMS} = 54.5 \text{ A} \quad (3.6)$$

With the results found in (3.4) – (3.6), the following Table 3.3 can be drawn.

Table 3.3. FES Converter Electrical Specifications

	Input Side (RMS Values)	***Output Side (DC Values)***
Grid Voltage (V)	220	600
Grid Current (A)	54.5	51.25
Real Power (kW)	34.17	30.75

3.3.3 FES Design Parameters

After the supercapacitor has provided the battery with 10% of its required energy, the remaining 90% will be provided by the FES and the grid simultaneously. This phase will not last more than 10 minutes of the battery charging process (see Chapter 5). Thus the maximum output energy provided by the FES is found as follows:

$$E_{FES,max} = 0.9 \cdot E_{O,max} - \frac{1}{6} \cdot P_{Grid} = 0.9 \text{ x } 11.25 - 30/6 = 5.125 \text{ kWh}$$

However since the FES is interfaced with the charging station dc bus via an IGBT converter:

$$ή = \frac{E_{FES,out}}{E_{FES,in}} = 0.9 \Leftrightarrow E_{FES,in} = \frac{E_{FES,out}}{0.9} = \frac{5.125}{0.9} \Leftrightarrow E_{FES,in} = 5.69 \text{ kWh} \quad (3.7)$$

The relation relating the FES moment of inertia to its rated speed (see Section 1.2.10, equation (1.7)) to provide the energy $E_{FES,in}$ is reminded below:

$$E = \frac{1}{2} \cdot J \cdot \omega^2$$

Table 3.4 below displays the available options for choosing an appropriate moment of inertia with the required rated speed to fulfill condition (3.7):

Table 3.4. FES Options (for $E_{FES,\ in}$ = 5.69 kWh)

Inertia Moment ($kg.m^2$)	5	10	25	50	75
Rated Speed (rpm)	27335	19330	12225	8645	7060

An FES with a DC voltage interface of 600 V and with applications in power sources has a typical speed ranging from 10000 to 15000 rpm [58]. Thus, an acceptable option for the FES choice is the third one in Table 3.4 above.

If the flywheel has a mass m (in kg) and a radius r (in m) then J is found as follows:

$$J = m \cdot r^2$$

Flywheels having the mentioned power (34 kW) and energy (5.7 kWh) specifications have a typical mass of 100 kg [82]. Therefore the radius is found as:

$$r = \sqrt{\frac{J}{m}} = \sqrt{\frac{25}{100}} \Leftrightarrow r = 0.5 \text{ m} \tag{3.8}$$

With Table 3.4 and (3.7)-(3.8) information, Table 3.5 below displays an option for the flywheel parameters choice to obtain the maximum energy required in the charging station design.

Table 3.5. Flywheel Parameters (for $E_{FES,\ in}$ = 5.69 kWh)

r (in m)	***J (in $kg.m^2$)***	***m (kg)***	***Speed (rpm)***
0.5	25	100	12225

3.4 Supercapacitor Converter

Like any conventional capacitor, a supercapacitor charges and discharges in a DC environment [66]. The interface here is thus between DC quantities, and a bidirectional chopper is required to allow both charging and discharging of the supercapacitor.

3.4.1 Converter Design

In order too allow bidirectional power flow, a buck-boost converter is necessary [19]. The switch technology chosen for such a converter is again the IGBT since it gives the converter a minimum efficiency of 90% [58] and it is fully controllable [19].

The control technique used is again PWM, but in this case, the control signal is almost constant and the carrier is a sawtooth signal (most commonly used) [19]. The supercapacitor converter is shown in Figure 3.2.

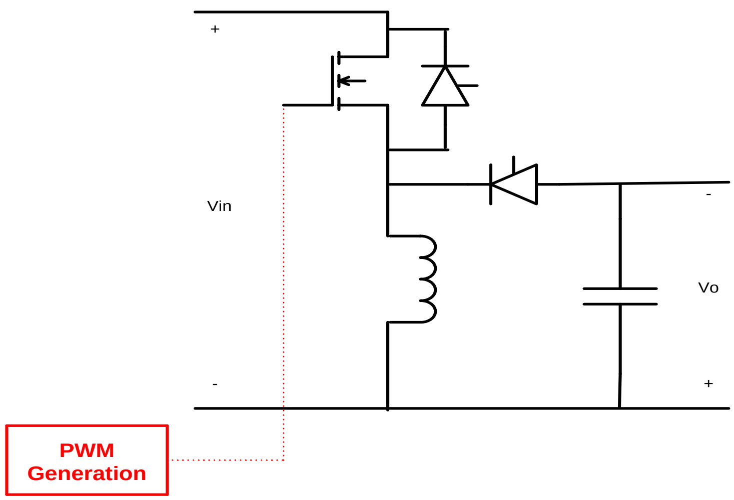

Figure 3.2. Supercapacitor Bidirectional Chopper

3.4.2 Charging Station Supercapacitor

The supercapacitor is required to provide the battery with 10% of its required energy during the beginning of the battery charging process (see Chapter 5). Thus, the maximum output energy provided by the supercapacitor is found as follows:

$$E_{Scap,max} = 0.1 \cdot E_{O,max} = 0.1 \text{ x } 11.25 = 1.125 \text{ kWh}$$

However, since the supercapacitor is interfaced with the charging station dc bus via an IGBT converter, the efficiency will play a role:

$$\acute{\eta} = \frac{E_{Scap,out}}{E_{Scap,in}} = 0.9 \Leftrightarrow E_{Scap,in} = \frac{E_{Scap,out}}{0.9} = \frac{1.125}{0.9} \Leftrightarrow E_{Scap,in} = 1.25 \text{ kWh} \tag{3.9}$$

The relation relating the supercapacitor moment capacitance to its rated voltage (see Section 1.2.10, equation (1.8)) to provide the energy $E_{Scap,in}$ is reminded below:

$$E = \frac{1}{2} \cdot C \cdot U^2$$

Table 3.6 below displays the available options for choosing an appropriate capacitance with the required voltage to fulfill condition (3.9):

Table 3.6. Supercapacitor Options (for $E_{Scap,\,in}$ = 1.25 kWh)

Capacitance (F)	100	150	200	250	300
Rated Voltage (V)	300	245	212.13	190	173.20

An acceptable option would be a series / parallel combination of supercapacitors whose resulting capacitance and voltage are 150 F and 245 V, respectively.

3.4.3 Electrical Specifications

The supercapacitor is rated to provide a maximum output power of 13.5 kW (see Chapter 5). With a DC bus voltage of 600 V, the output current on the DC side is:

$$I_{DC} = \frac{P_{DC}}{V_{DC}} = \frac{13\,500}{600} \Leftrightarrow I_{DC} = 22.5 \text{ A} \tag{3.10}$$

Since the supercapacitor is interfaced with the charging station DC bus via an IGBT converter, the input DC power must be:

$$ή = \frac{P_{DC}}{P_{AC}} = 0.9 \Leftrightarrow P_{AC} = \frac{P_{DC}}{0.9} = \frac{13.5}{0.9} = 15 \text{ kW} \tag{3.11}$$

In the previous section, it has been found that the supercapacitor must be rated less than 245 V in order to provide the required energy during the vehicle battery charging process. The supercapacitor rated current can now be found as follows:

$$P_{Scap,in} = V_{Scap,in}.I_{Scap,in} \Leftrightarrow I_{Scap,in} = \frac{P_{Scap,in}}{V_{Scap,in}} = \frac{15000}{245} = 61.25 \text{ A} \tag{3.12}$$

With the information (3.9)-(3.12), Table 3.7 below displays the supercapacitor converter electrical specification.

Table 3.7. Supercapacitor Converter Electrical Specifications

	Input Side (DC Value)	Output Side (DC Value)
Supercapacitor Voltage (V)	245	600
Supercapacitor Current (A)	61.25	22.5
Power (kW)	15	13.5

3.5 Output Converter

In order to adapt to various battery car voltages, the charging station dc bus must be interfaced with the battery via a generic DC/DC converter that must also be bidirectional to allow both of the battery charging and V2G modes.

3.5.1 Converter Design

The output converter configuration looks exactly like the one shown in Figure 3.2 above. Since the dc bus voltage is always higher than the battery voltage, the converter acts as a buck configuration in battery charging mode, and as a boost configuration in V2G mode.

3.5.2 Electrical Specifications

The output converter input current is equal to the sum of the output currents of the three previously mentioned converters:

$$I_{total,DC} = I_{Grid,DC} + I_{FES,DC} + I_{Scap,DC}$$
$$\Leftrightarrow I_{total,DC} = 50 + 51.25 + 22.5 = 123.75 \text{ A} \quad (3.13)$$

The converter input power is calculated as follows:

$$P_{total,in} = V_{DC}.I_{total,DC} = 600 \text{ x } 123.75 = 74.25 \text{ kW} \quad (3.14)$$

The converter output power is calculated as follows:

$$\acute{\eta} = \frac{P_{out}}{P_{in}} = 0.9 \Leftrightarrow P_{out} = \acute{\eta}.P_{in} = 0.9 \text{ x } 74.25 = 67 \text{ kW} \quad (3.15)$$

The converter output voltage is the maximum PHEV battery voltage, which is 270 V (Table 2.1).

Finally the converter output current is calculated as follows:

$$I_{out} = \frac{P_{out}}{V_{out}} = \frac{67000}{270} = 248 \text{ A} \tag{3.16}$$

With the information (3.13)-(3.16), the following Table 3.8 which displays the charging station output converter electrical specification can be drawn.

Table 3.8. Charging Station Output Converter Electrical Specifications

	Input Side (DC Value)	***Output Side (DC Value)***
Voltage (V)	600	270
Current (A)	123.75	248
Power (kW)	74.25	67

3.6 Complete Power Circuit

The present section describes the combined design of the charging station, and then lists its electrical specifications.

3.6.1 Circuit Design

The electrical grid, the supercapacitor, and the FES are all interfaced via their respective power electronic converters previously designed to a common dc bus. The interface with the PHEV battery is also done via a bidirectional DC/DC converter (see Section 3.5).

3.6.2 Electrical Specifications

The energy and power requirements of each current source are summarized in Table 3.9 below:

Table 3.9. Charging Station Electrical Specifications

	Electrical Grid	***FES***	***Supercapacitor***
Maximum output energy (kWh)	5.56	5.70	1.25
Converter Efficiency (%)	0.9	0.9	0.9
Maximum output energy (kWh)	5	5.125	1.125
Maximum time of charging operation (min)	10	10	5
Maximum Output power (kW)	30	30.75	13.5

Figure 3.3 below displays the combined charging station power circuit.

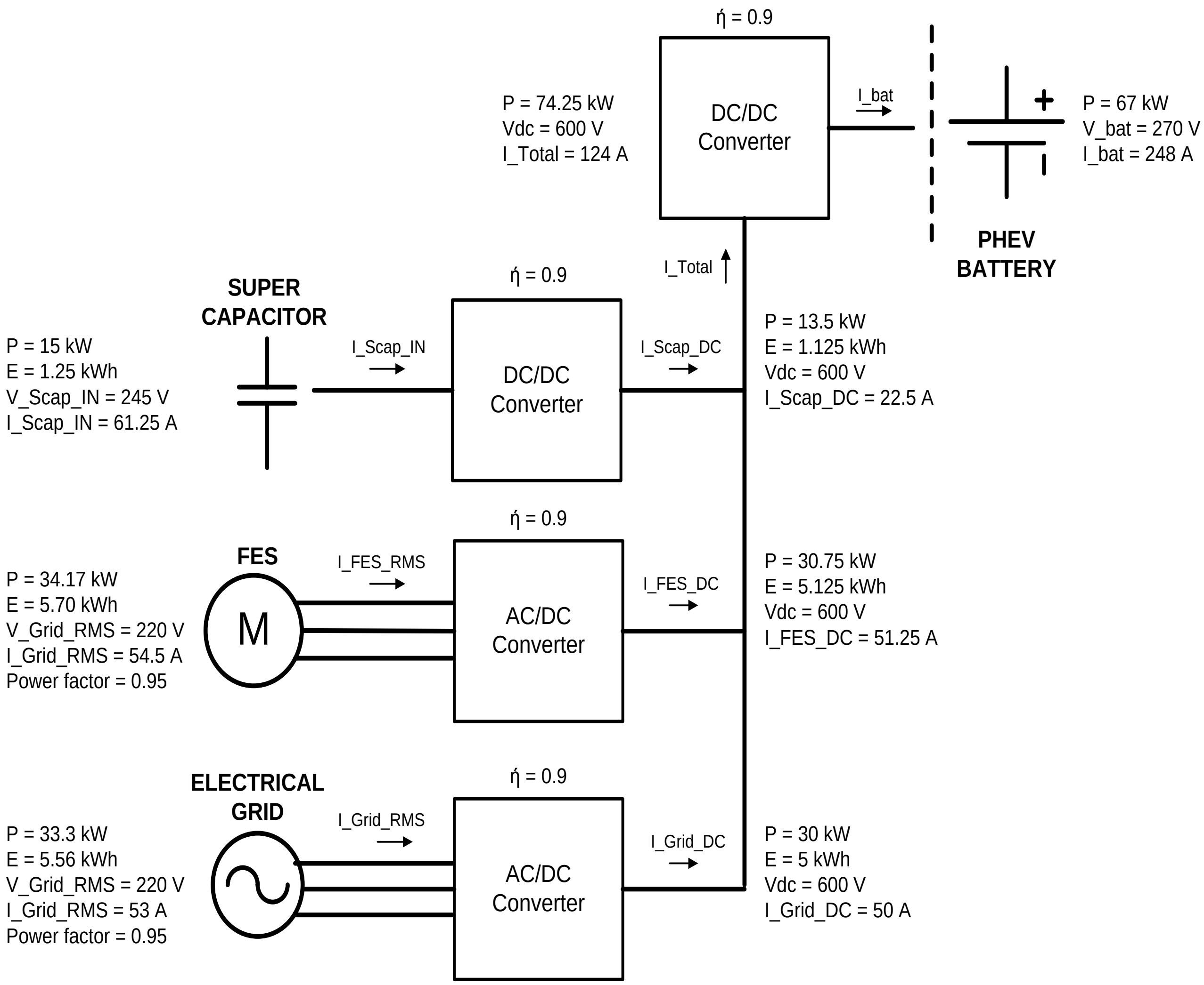

Figure 3.3. Charging Station Power Circuit

CHAPTER 4
Charging Station Control Circuit

In the previous chapter, the power circuit has been designed along with its electrical specifications. The present chapter explains the control of each individual converter, then the whole charging station control circuit.

4.1 Converters Individual Control

This section elaborates on the individual control schemes of each of the four charging station power electronic converters.

4.1.1 Grid Converter Control

The grid side converter control circuit is shown in Figure 4.1 below. It is composed of two nested control loops:

The outer loop is for voltage regulation. In order to keep the output dc bus voltage constant, the error between the reference DC voltage and the measured bus voltage is fed to a PI voltage controller that produces as an output the reference DC grid current.

The inner loop regulates the output DC current, whose reference is the output of the previous outer loop. The error between the reference and measured DC current is fed to a current regulator whose output is sent to the grid converter switching scheme (PWM).

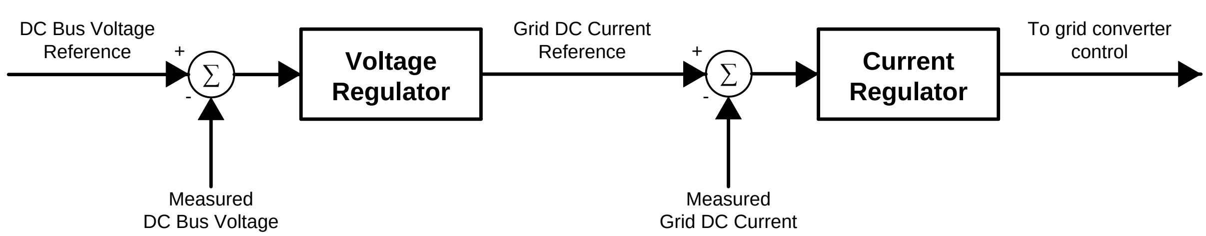

Figure 4.1. Grid Converter Control

4.1.2 FES Control

The FES control by itself is difficult.

4.1.2.1 FES Emulation

It has been demonstrated that an FES could easily be emulated by a PMDC (Permanent Magnet DC Machine) [83]. Such operation would considerably decrease the system size and cost [83]. The FES system model will thus be replaced by a DC machine model as shown in Figure 4.2.

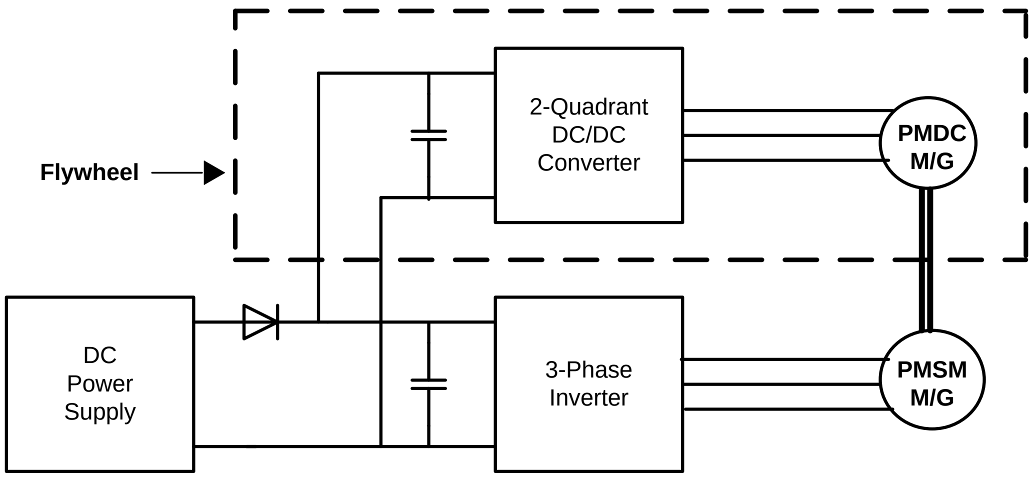

Figure 4.2. Flywheel Emulation Using a PMDC [Based on 83]

The power flow in the above system is bidirectional. Every power transfer is done through the permanent magnet synchronous machine (PMSM), which can act as motor and generator. The DC power supply not only imposes the dc bus voltage, but it also compensates for the system losses.

It is reminded that the kinetic energy dW (in J) stored in the above system with moment of inertia J_F (in $Kg.m^2$) and rotating from one speed ω_1 to another speed ω_2 (in rad/s) is expressed as [83]:

$$dW = \frac{1}{2} \cdot J_F \cdot (\omega_2^2 - \omega_1^2)$$

The above system is designed to operate in three modes based on the stored energy using the above formula: charging, discharging, and no charging [83]. Each model is now explained below.

In the charging mode, the power flows from the dc bus to the PMDC through the PMSM. In such a case the DC machine is accelerated from the speed ω_1 to a higher speed ω_2.

In the discharging mode, the power flows from the PMDC to the dc bus through the PMSM. In such a case, the DC machine is decelerated from the speed ω_2 to a lower speed ω_1.

In the no charging mode, the DC machine runs at a constant at speed, and there is thus no power flow.

4.1.2.2 System Control

The amount of energy transferred in or out of the flywheel can be controlled by controlling the PMSM torque by imposing either a positive or negative torque command in the PMSM controller, which is based on field orientated control (FOC) in a rotor frame.

Under ideal FOC, i_{ds}^r is set to 0 and the PMSM electromagnetic torque τ_{E_SM} can then be written as [84]:

$$T_{E\_SM} = \frac{3}{2}.\frac{p}{2}.\lambda_{af} i_{qs}^r \tag{4.1}$$

where λ_{af} is the rotor flux linkages, i_{qs}^r is the torque component of the stator current in the rotor reference frame, and p is the number of pole pairs.

The relationship between i_{qs}^r and i_{FW} (Flywheel transfer current to/from the inverter) is found from the steady-state power balance between the dc power going into the inverter and the ac power going into the PMSM [83]. If we neglect the inverter losses, we have:

$$P_{inv} = P_{SM}$$

$$\Leftrightarrow i_{FW}.V_{DC} = \tau_{E\_SM}.\omega_m \tag{4.2}$$

Substituting the electromagnetic torque expression (4.1) into the power balance relation (4.2) and solving for i_{qs}^r, we get the following relation (which is also the flywheel control algorithm for both charging and discharging modes):

$$I_{qs}^* = \frac{4.V_{DC}}{3p\omega_{m.}\ \lambda_{af}} \cdot i_{FW} \tag{4.3}$$

Figure 4.3 below displays the FES control loop according to the above relation. At start-up, the control algorithm starts the PMSM using an initiation algorithm. The PI current controller is used to maintain the power flow.

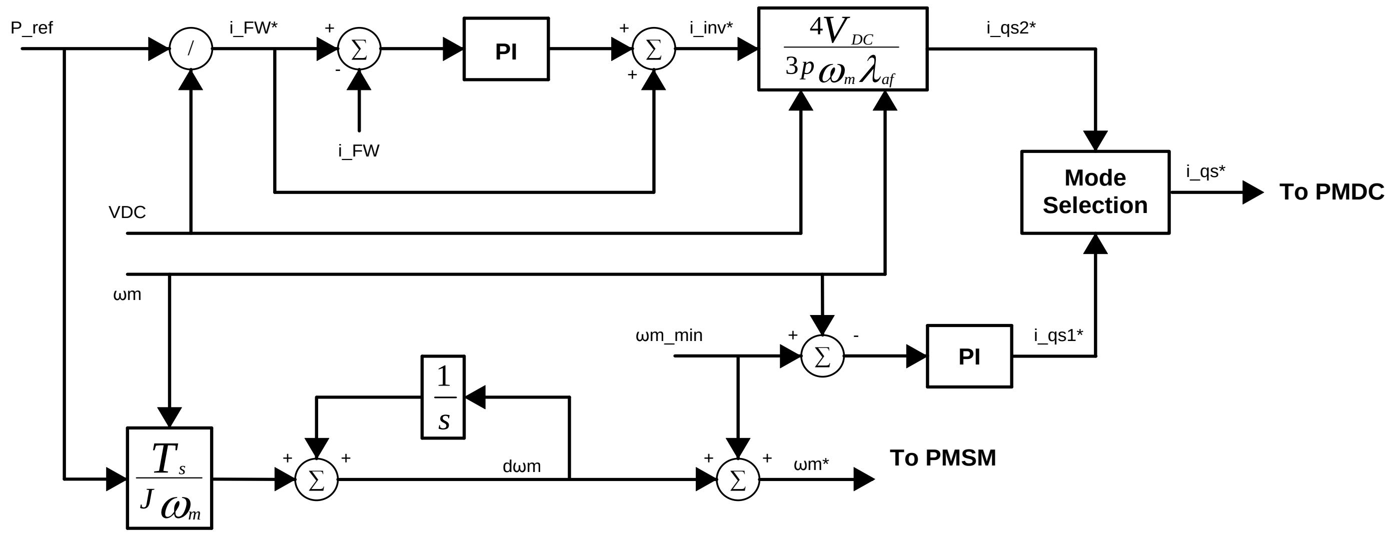

Figure 4.3. Flywheel Charging and Discharging Control [Based on 83]

4.1.3 Supercapacitor Converter Control

The supercapacitor control design is analogous to the flywheel control design shown in Figure 4.3 above and is designed to allow charging and discharging of the supercapacitor. Figure 4.4 below illustrates such control.

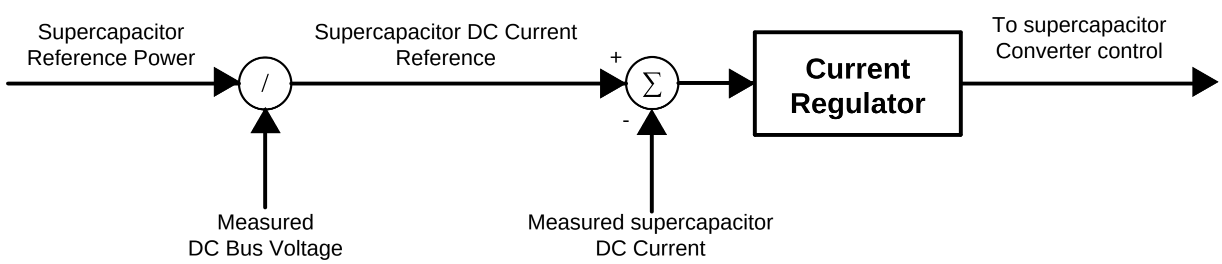

Figure 4.4. Supercapacitor Converter Control

The DC/DC converter output current reference is produced by dividing the reference supercapacitor's required power by the dc bus voltage.

The error in current is then fed to a PI current regulator in order to maintain the power flow between the charger dc bus and the supercapacitor. Finally the regulator output will be directed to the supercapacitor control scheme. The mode of operation (charging or discharging mode) depends on the sign of the supercapacitor's reference power.

4.1.4 Charging Station Output Converter Control

The control scheme of the output converter is very similar to the grid converter control, and is presented in Figure 4.5 below. It is composed of two nested control loops:

The outer control loop is designed for voltage regulation. The error between the battery nominal reference voltage and the measured battery charging voltage is fed to a PI controller, whose output is the battery charging current reference.

The inner loop regulates the battery charging current. The reference here is the output of the previous outer loop. The error between the reference and the measured current is also fed to a PI controller whose output is sent to the charging station output converter control scheme.

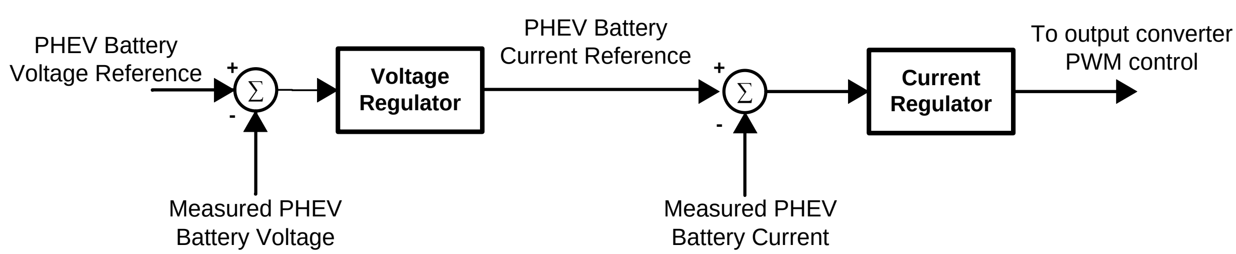

Figure 4.5. Charging Station Output Converter Control

4.2 Control Circuit Design

This section presents an algorithm that combines the previous individual controls in such that it minimizes the PHEV battery charging duration.

4.2.1 Charging Station Central Control

A charging station cycle is composed of a PHEV battery charging period (two phases) that does not exceed 15 minutes, followed by a period (one phase) during which the storage devices are fully recharged, which lasts a maximum of 7.5 minutes. This is demonstrated in Figure 4.6.

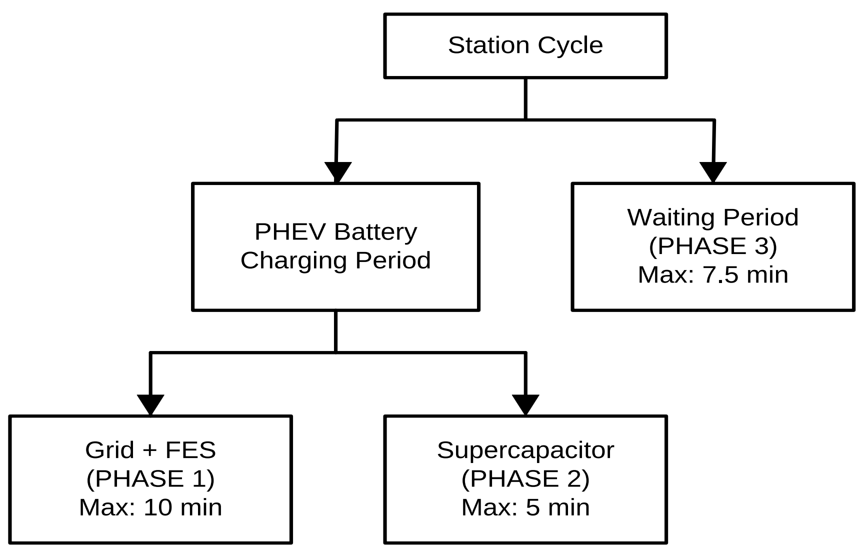

Figure 4.6. Schematic Diagram of the Charging Station Cycles

More details on the three phases will be provided in the next chapter.

4.2.2 Central Control Algorithm

In order to obtain the requirements of Figure 4.6, the algorithm of Figure 4.7 below is proposed. Table 4.1 displays the abbreviations used in the flowchart in Figure 4.7. Blue and red instructions indicate whether energy is being transferred from the charger to the battery, or from the grid to the storage devices (to recharge them), respectively.

Table 4.1. Figure 4.7 Abbreviations

Abbreviations	SC	FES	C_act	C
Expressions	supercapacitor	flywheel	Actual battery capacity	Total battery capacity

In standby mode, there is no PHEV battery connected to the charging station, and the energy storage devices have been fully recharged. At this moment, the FES rotates at constant speed Ω_o (see Section 4.1.2) and thus there is no power transfer (dW = 0). The supercapacitor voltage continues to increase asymptotically to its rated voltage, whereas its current tends asymptotically to 0. The charging station remains in this mode until the arrival of a PHEV at the station.

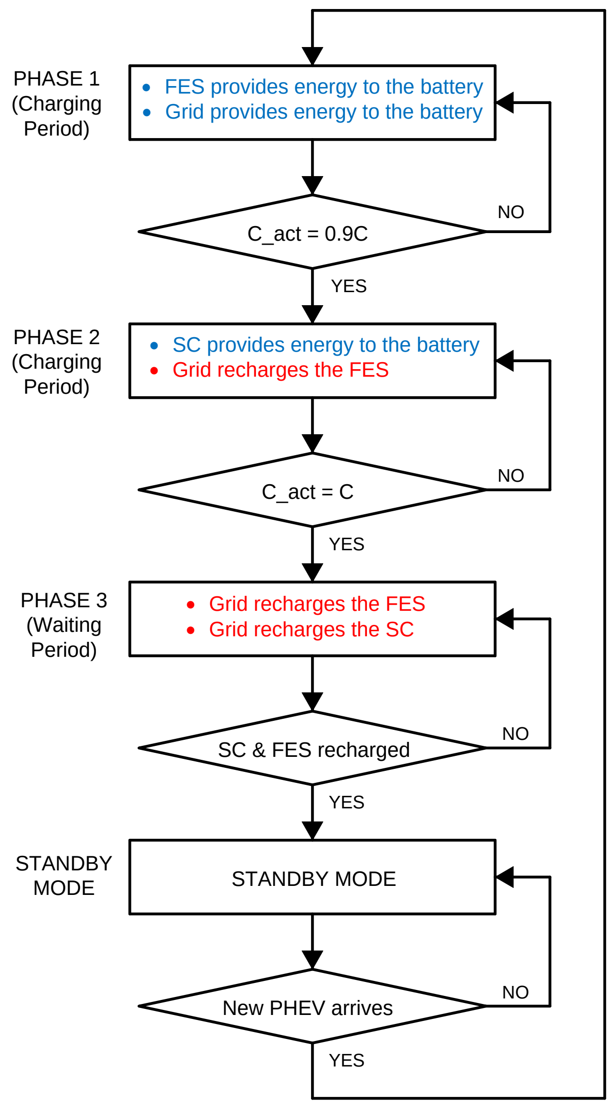

Figure 4.7. Central Control Algorithm Flowchart

CHAPTER 5
Charging Station Operation

The charging station operates as described in the flowchart shown in Figure 4.7. The energy management of the energy sources is done via optimization; the topic of this chapter. Two examples will be used to illustrate such operation.

5.1 Charging Time Minimization

The charging station is designed to minimize the PHEV battery charging time and required duration to recharge the storage devices. This requires an effective management strategy of the charging stations' energy sources: grid, supercapacitor, and FES.

5.1.1 Charging Station Cycle

As mentioned previously, a charging station cycle is composed of three phases. The order of Phases 1 and 2 has been established by considering the fact that some PHEV users may have a limited amount of time to spend at the charging station; for this reason, most of the PHEV battery charging is done in the beginning of the cycle (Phase 1). The maximum duration of each phase has been determined by optimization (further details on the order of the charging durations of the FES and supercapacitor were provided in section 2.3.2).

- Phase 1: The FES and the electrical grid provide energy to the PHEV battery until it reaches 90% of its required capacity. The maximum duration of this phase is 10 minutes.
- Phase 2: While the supercapacitor provides energy to the PHEV battery until it reaches its required capacity, the electrical grid is recharging the FES with a capacity determined by optimization (described in Section 5.1.3). The maximum duration of this phase is 5 minutes.
- Phase 3: During this phase, which lasts no more than 7.5 minutes, the electrical grid is recharging the supercapacitor and the FES to their respective full capacities. It is also called the "waiting period" because, during this time, no PHEV battery is allowed to be connected to the charging station.

Once the storage devices are fully recharged, the charging station enters its standby mode until another PHEV arrives at the charging station to recharge its battery. Examples of the system operation are provided in Section 5.2.

5.1.2 Problem Formulation

A charging station cycle is graphically represented in Figure 5.1, where:

- Blue and red colors indicate whether energy is being transferred from the charger to the battery, or from the grid to the storage devices (to recharge them), respectively.
- Positive and negative quantities indicate whether energy is being delivered or absorbed by the device, respectively.
- P and C denote the grid power and the PHEV battery capacity, respectively.

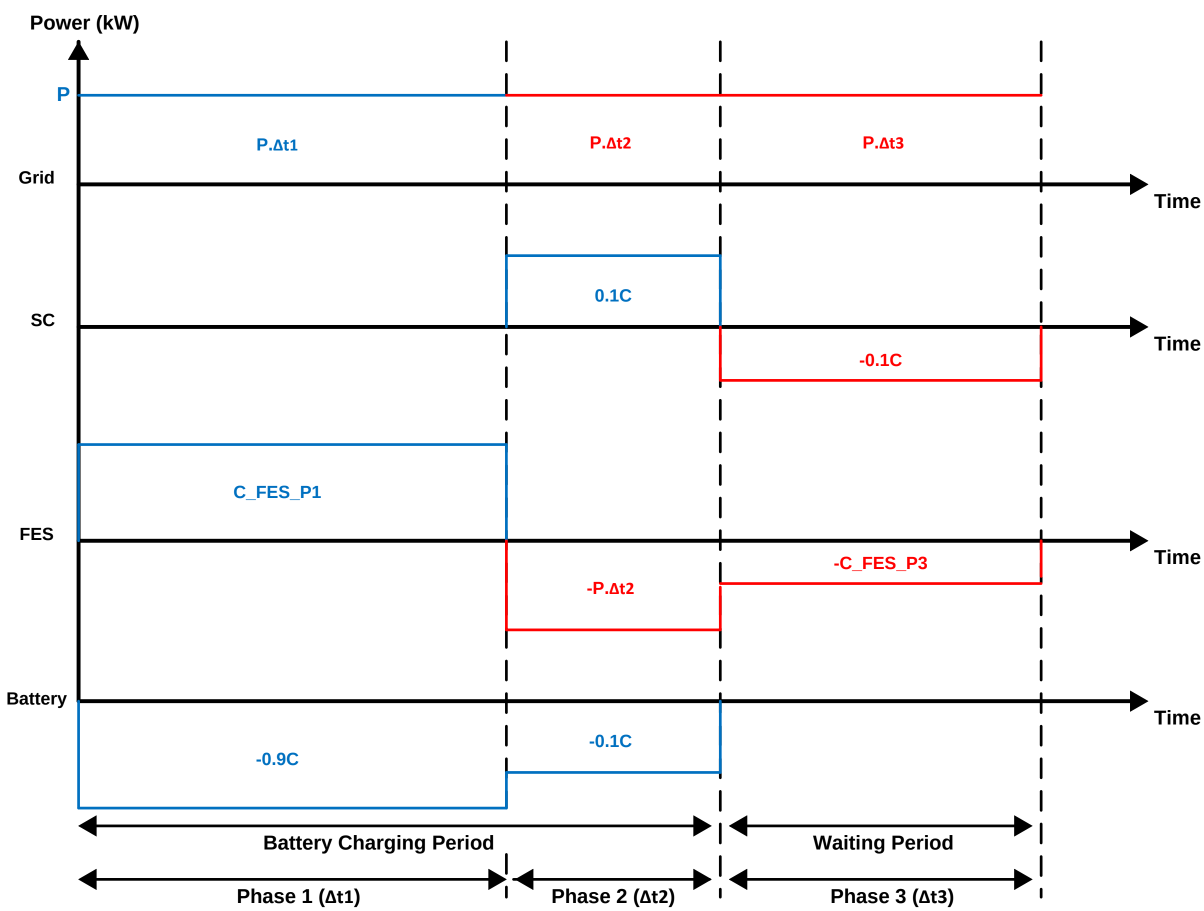

Figure 5.1. Detailed Charging Station Cycle

While the grid provides 5 kWh of the maximum charging station output energy of 11.25 kWh (see Table 2.3) during Phase 1, the storage devices provide the remaining 6.25 kWh as follows: 1.125 kWh is provided from the supercapacitor during Phase 2, and 5.125 kWh is provided from the FES during Phase 1.

The choice of such proportions is in accordance with the station's storage devices characteristics (see Section 2.3.2): the supercapacitor is in operation for a relatively small period (maximum of 5 minutes) compared to the FES operation duration (maximum 10 minutes).

Once a PHEV arrives at the charging station, the parameters in Figure 5.1 that need to be computed are listed in Table 5.1 below.

Table 5.1. Optimization Parameters

Parameter Name	Phase 1 Duration (min)	Phase 2 Duration (min)	Phase 3 Duration (min)	FES capacity in phase 1 (kWh)	FES capacity in phase 3 (kWh)
Symbolic Notation	Δt_1	Δt_2	Δt_3	C_{FES-P1}	C_{FES-P3}
Variable Maximum	10	5	7.5	5.125	5.125

The problem can be written as:

$$\min f(\underline{x}) = \sum_{i=1}^{3} x_i$$

$$\text{with } \underline{x} = [\Delta t_1 \quad \Delta t_2 \quad \Delta t_3 \quad C_{FES-P1} \quad C_{FES-P3}]^T \tag{5.1}$$

The constraints imposed on such function are of equality and inequality types. They can be easily visualized in Figure 5.1.

- Since the supercapacitor's capacity is smaller than the capacity of the FES, the duration of Phase 2 must be smaller than the duration of Phase 1:

$$\Delta t_2 < \Delta t_1 \tag{5.2}$$

- The waiting period must never exceed the charging period, because the waiting time must be minimized to satisfy the clients' needs.

$$\Delta t_3 < \Delta t_1 + \Delta t_2 \tag{5.3}$$

- The maximum of each parameter is displayed in table 5.1.

- As already mentioned, in Phase 1, the FES and the grid (who delivers a power, p, in kW) are recharging the PHEV battery to 90% of its required capacity, C.

$$p.\Delta t_1 + C_{FES\text{-}P1} = 0.9.C \tag{5.4}$$

- In Phase 3, the grid is recharging the supercapacitor and the FES:

$$p.\Delta t_3 - C_{FES\text{-}P3} - 0.1C = 0 \tag{5.5}$$

- The FES is providing energy to the PHEV battery during Phase 1, and is being recharged by the grid during Phases 2 and 3:

$$C_{FES\text{-}P1} - p.\Delta t_2 - C_{FES\text{-}P3} = 0 \tag{5.6}$$

5.1.3 Problem Summary

The optimization function (5.1), combined with the constraints in (5.2) to (5.6), produces the charging station optimization problem that can be written as follows:

$$f(\underline{x}) = \sum_{i=1}^{3} x_i \tag{5.7}$$

With:

- Variables:

$$\underline{x} = [\Delta t_1 \quad \Delta t_2 \quad \Delta t_3 \quad C_{FES-P1} \quad C_{FES-P3}]^T$$

- Equality Constraints:

$$A_{eq}.\underline{x} = \underline{b_{eq}} \Leftrightarrow \begin{bmatrix} p & 0 & 0 & 1 & 0 \\ 0 & 0 & p & 0 & -1 \\ 0 & -p & 0 & 1 & -1 \end{bmatrix} \cdot \begin{bmatrix} \Delta t_1 \\ \Delta t_2 \\ \Delta t_3 \\ C_{FES-P1} \\ C_{FES-P3} \end{bmatrix} = \begin{bmatrix} 0.9C \\ 0.1C \\ 0 \end{bmatrix}$$

- Inequality Constraints:

$$A.\underline{x} < \underline{b} \Leftrightarrow \begin{bmatrix} -1 & 1 & 0 & 0 & 0 \\ 0 & 1 & -1 & 0 & 0 \\ -1 & -1 & 1 & 0 & 0 \end{bmatrix} \cdot \begin{bmatrix} \Delta t_1 \\ \Delta t_2 \\ \Delta t_3 \\ C_{FES-P1} \\ C_{FES-P3} \end{bmatrix} < \begin{bmatrix} 0 \\ 0 \\ 0 \end{bmatrix}$$

- Lower and Upper Bounds:

$$\underline{\text{lb}} < \underline{x} < \underline{\text{up}} \Leftrightarrow \begin{bmatrix} 0 \\ 0 \\ 0 \\ 0 \\ 0 \end{bmatrix} < \begin{bmatrix} \Delta t_1 \\ \Delta t_2 \\ \Delta t_3 \\ C_{FES-P1} \\ C_{FES-P3} \end{bmatrix} < \begin{bmatrix} 10 \\ 5 \\ 7.5 \\ 5.125 \\ 5.125 \end{bmatrix}$$

5.2 Charging Station Operation

The charging station operates as shown in the flowchart of Figure 4.7.

Energy management parameters are given in tables 5.3, 5.5A, and 5.5B, where:

- Blue and red numbers indicate whether energy is being transferred from the charger to the battery, or from the grid to the storage devices (to recharge them), respectively.
- Positive and negative quantities indicate whether energy is being delivered or absorbed by the device, respectively.

The following battery charging characteristics are displayed in Figures 5.2 and 5.4:

- Battery SOC (in %)
- Battery current (in A)
- Battery voltage (in V)

The following charger characteristics are displayed in Figures 5.3 and 5.5:

- FES speed (in rad/s)
- Grid current (in A)
- FES current (in A)
- Supercapacitor current (in A)
- Total current (in A): The sum of the grid, FES, and supercapacitor currents
- Supercapacitor voltage (in V)

5.2.1 Charging of a Single PHEV Battery

This scenario considers a single PHEV battery being recharged by the charging station. Its technical specifications are presented below:

Table 5.2. PHEV Battery Specifications

Total Battery Capacity (kWh)	***Battery Initial & Final SOCs (%)***	***Required Battery Capacity (kWh)***	***Battery Nominal Voltage (V)***	***Battery Maximum Charging Voltage (V)***	***Battery Minimum Charging Voltage (V)***	***Battery Maximum Charging Current (A)***
12	20 to 95	9.75	200	233.2	166.5	300

The energy management that will minimize the charging phase duration and the waiting phase duration for this PHEV battery is displayed in Table 5.2 below.

Table 5.3. Charger Energy Management for the PHEV Battery

	Complete Cycle			
	Charging Period		***Waiting Period***	
	Phase 1	***Phase 2***	***Phase 3***	***Total***
Duration (min)	10	4	4	18
Grid Energy (kWh)	5	2	2	9
SC Energy (kWh)	0	0.9	-0.9	0
FES Energy (kWh)	3.1	-2	-1.1	0
Battery Energy (kWh)	**-8.1**	**-0.9**	**0**	**9**

The evolution of the PHEV battery parameters are displayed in Figure 5.2.

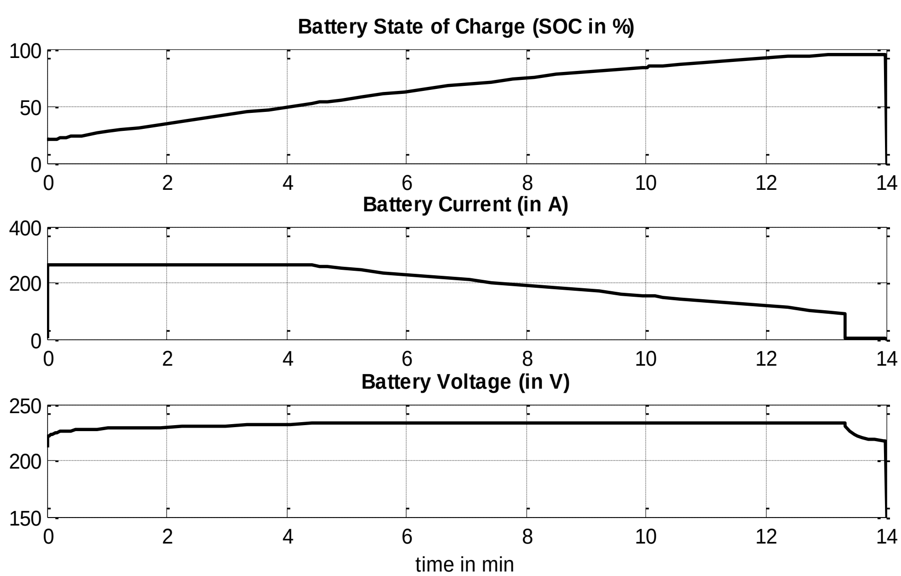

Figure 5.2. PHEV Battery Characteristics Evolution

Figure 5.3 displays the evolution of the charger's parameter during the full cycle of the charging period.

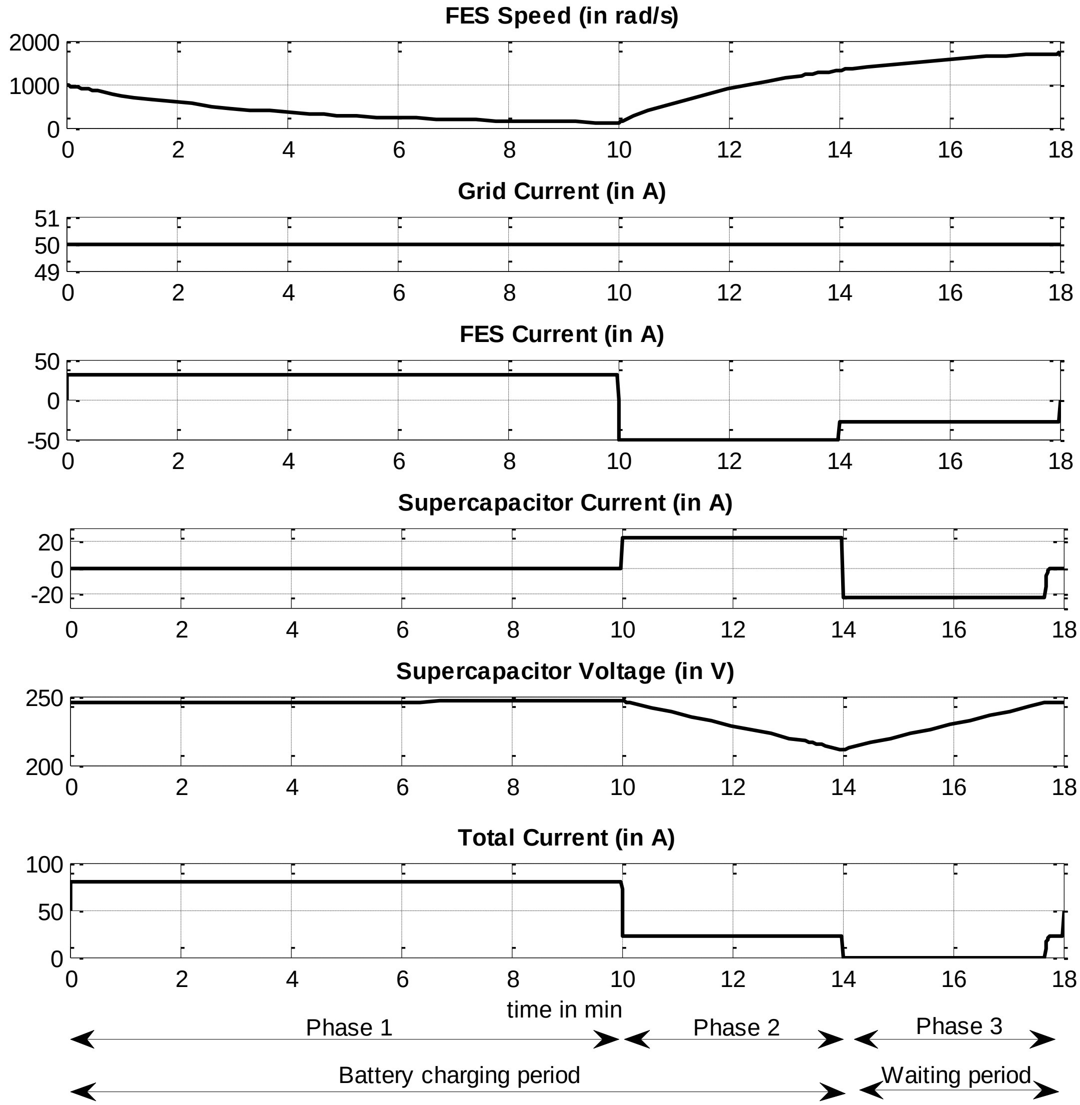

Figure 5.3. Evolution of the Charger's Parameters during the Full Cycle

5.2.2 Charging of Two Consecutive PHEV Batteries

This scenario considers two PHEV batteries that are consecutively recharged by the charging station. Their respective technical specifications are presented below:

Table 5.4. PHEV Batteries Specifications

	Total Battery Capacity (kWh)	Battery Initial & Final SOCs (%)	Required Battery Capacity (kWh)	Battery Nominal Voltage (V)	Battery Maximum Charging Voltage (V)	Battery Minimum Charging Voltage (V)	Battery Maximum Charging Current (A)
Battery 1	15	25 to 90	9.75	200	233.2	166.5	300
Battery 2	13	30 to 95	8.45	180	210	150	280

The energy management scheme that will minimize the charging durations of both battery vehicles is displayed in Tables 5.3 and 5.4.

Table 5.5A. Charger Energy Management for Battery 1:

	Complete Cycle			
	Charging Period		***Charging Period***	
	Phase 1	***Phase 2***	***Phase 3***	***Total***
Duration (min)	10	4.75	4.75	19.5
Grid Energy (kWh)	5	2.375	2.375	9.75
SC Energy (kWh)	0	0.975	-0.975	0
FES Energy (kWh)	3.775	-2.375	-1.4	0
Battery Energy (kWh)	**-8.775**	**-0.975**	**0**	**9.75**

Table 5.5B. Charger Energy Management for Battery 2:

	Complete Cycle			
	Charging Period		***Charging Period***	
	Phase 1	***Phase 2***	***Phase 3***	***Total***
Duration (min)	10	3.45	3.45	16.9
Grid Energy (kWh)	5	1.725	1.725	8.45
SC Energy (kWh)	0	0.845	-0.845	0
FES Energy (kWh)	2.605	-1.725	-0.88	0
Battery Energy (kWh)	**-7.605**	**-0.845**	**0**	**8.45**

The respective PHEV battery characteristics' evolutions are displayed in Figure 5.4.

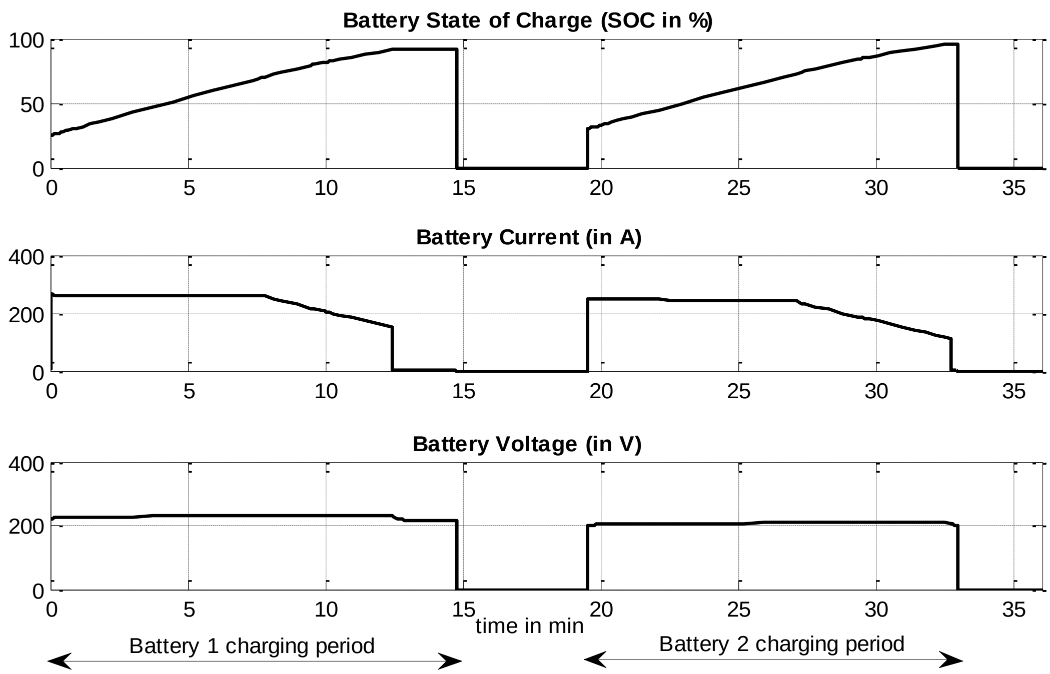

Figure 5.4. Batteries 1 and 2 Characteristics Evolution
during the Charging Phases

Figure 5.5 displays the evolution of the charger characteristics during the full cycle of the charging station.

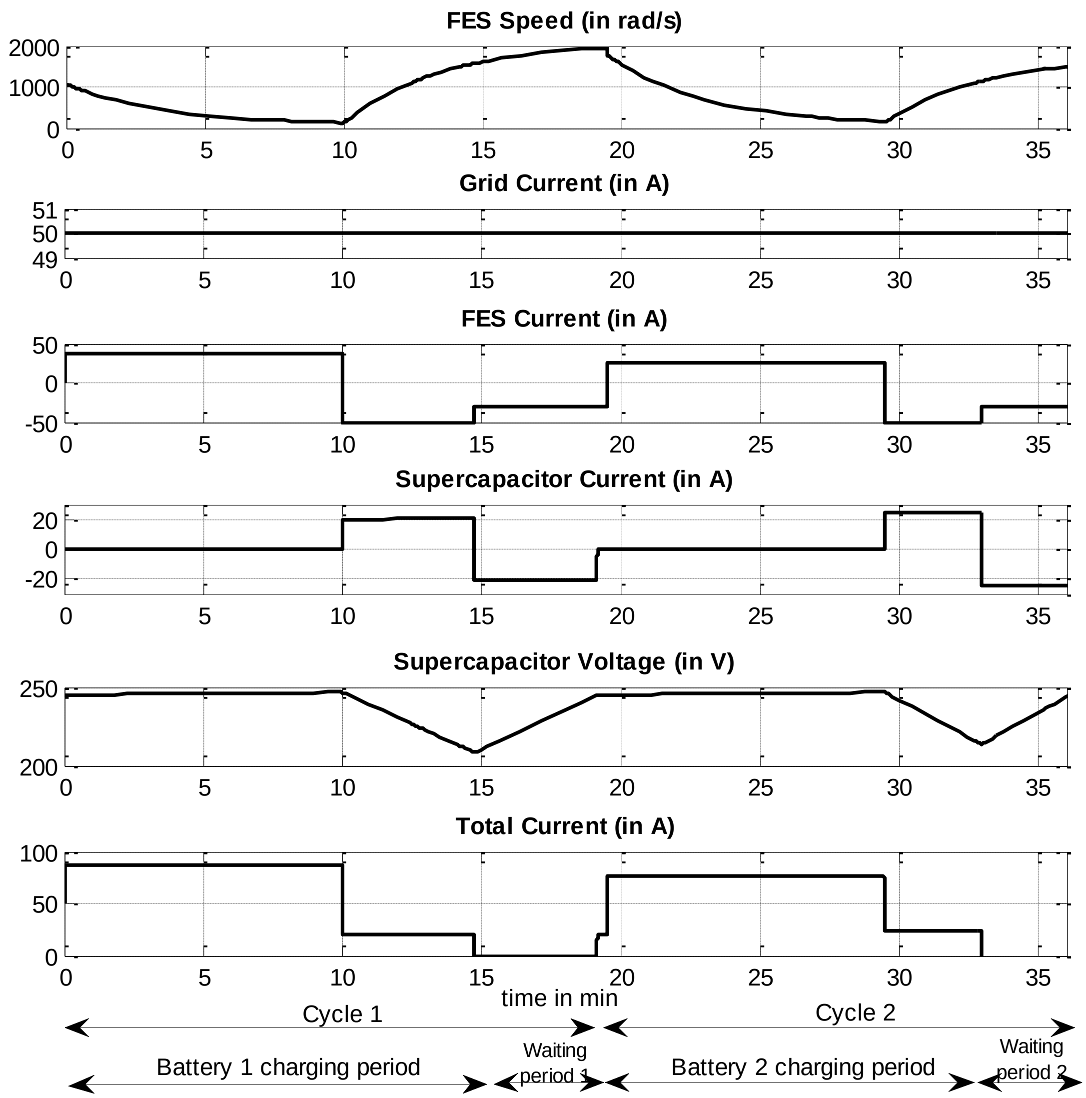

Figure 5.5. Charger Characteristics during the Two Cycles

CHAPTER 6
Conclusion

This chapter presents a summary of the work conducted in the research, and lists some recommendations for future work to be done on this topic.

6.1 Summary

In this thesis, the basic configuration used for the design of the fast charging station (including energy requirements and storage devices choice) has been described, the different power electronic interfaces have been designed, and the individual control schemes of each converter as well as the control and proposed algorithm of the whole charging station have been presented. Afterwards the charging station operation has been simulated with two scenarios: the charging process of a single PHEV battery, and two consecutive PHEV batteries.

6.2 Conclusions

In this thesis, the design and simulation of a fast-charging station for PHEV batteries has been developed. The combination of a flywheel and a supercapacitor as additional stationary storage devices is an excellent option since it inherently has four advantages: high energy density, high power density, charging and discharging times in the order of minutes, and environmentally friendly. The developed algorithm efficiently manages the three station energy sources, and allows the charging of PHEV batteries whose capacities are below 15 kWh in a maximum duration of 15 minutes from 20% to 95% of their state-of-charge, and maximizes the waiting time (to recharge the storage devices) to 7.5 minutes when no PHEV is present at the station. Afterwards the station enters the standby mode, where the supercapacitor voltage remains constant and its current tends asymptotically to zero, while the flywheel rotates at constant speed. The reduction of the duration of the charging station operation will accelerate the battery recharging process in a battery swapping scheme.

6.3 Recommendations for Future Work

While a general control algorithm has been developed in this research to minimize the battery charging time and the duration required to charge the storage devices, more research could be conducted on the following topics:

- Optimization of the combination of flywheel and supercapacitor in terms of energy and power sizing.
- Impact of the battery charger on the power quality of the electric grid supply.
- Design of more efficient converter systems for the flywheel and supercapacitor charging schemes.

REFERENCES

[1] S.G. Wirasingha, A. Emadi, "Pihef: Plug-in Hybrid electric factor," in *Proc. 2009 IEEE VPPC'09 Conf.,* pp. 661-668.

[2] L. Dickerman, J. Harrison, "A new car, a new grid," *IEEE Trans. Power & Energy*, vol. 8, pp. 58-59, Apr. 2010

[3] *Electric Vehicle Conductive Charge Coupler*, SAE J1772, Recommended Practice, Draft Document in progress, 2009

[4] "Better Place partners to bring electric vehicles to Australia," *Better Place*. 2009 [Online]. Available: http://australia.betterplace.com/

[5] David Ehrlich, "The Electric Car Charging Startup Takes on its Biggest Project to Date." *Better Place to Charge up Australia* 2008. [Online] Available: http//cleantech.com/news/3761/batter-place-charge-Australia

[6] The Associated Press, "GM Unveils Volt Electric Car." *CBC.ca* 2008. [Online]. Available: http://www.cbc.ca/technology/story/2008/09/17GM-Volt.html

[7] J. Zhoua, P. Notten, "Studies on the degradation of Li-ion batteries by the use of micro reference electrodes," *IEEE Trans. Power Sources*, no. 177, p. 553-560, Nov. 2007.

[8] "PHEVs Going International: Europe's Avere Conference" *CalCars The California Cars Initiative – 100+ MPG Hybrids*. [Online]. Available: http://www.calcars.org/calcars-news/769.html

[9] "Mitsubishi EV Fast Recharge Station Open to Public" *Euro DB Automotive*. [Online]. Available: http://www.eurodb.com.au/New-used-car-review/mitsubishi/mitsubishi-ev-fast-recharge-station-open-to-public/

[10] "Electric Vehicle Fast Chargers - Level 3" *BTCPower*. [Online]. Available: http://www.btcpower.com/products-and-applications/electric-vehicle-chargers-level-3/

[11] "Powering Transportation with Renewable Energy Sources" *Eco-Trans Alliance*. [Online]. Available: http://www.ecotransalliance.com/ev-phev-chargers.html.

[12] "European Car of the Year – 2011" *Nissan*. [Online]. Available: http://www.nissan.ca/vehicles/ms/leaf/en/blog.aspx?item=0&title=European Car of The Year - 2011

[13] H. Oman, "Making battery last longer," in *IEEE Trans. AES System* vol. 14, pp. 19-21, Sep. 1999.

[14] B. Dickinson and J. Gill, "Issues and benefits with fast charging industrial batteries," in *Proc. 2000 IEEE Battery Conference on Applications and Advances*, pp. 223-229.

[15] P. Cheng and C. Chen, "A high-efficiency fast charger for lead-acid batteries," in *Proc. 2002 IEEE IECON 02*, pp. 1410-1415.

[16] J. Alvarez, J. Marcos, A. Lago, A. Nogueiras, J. Doval and C. M. Peiialver*,* "A fully digital smart and fast lead-acid battery charge system," in *Proc. 2003 IEEE Power Electronics Specialists Conf.,* pp. 913-917.

[17] *The Plug Standard Needed For Electric Car-Charging Cord Interface: SAE J1772*, SAE J1772 Standard, Apr. 2009. [Online]. Available: http://gm-volt.com/2009/04/16/plug-standard-needed-for-electric-car-charging-cord-interface-sae-j1772/.

[18] A. Rufer, "Today and tomorrow's meaning of power electronics within the grid interconnection," in *Proc. 2007 IEEE Power Electronics and Applications Conf.,* pp. 1-11.

[19] N. Mohan, Tore M. Undeland, William P. Robbins, "Classification of Power Processors and Converters," in *Power Electronics Converters, Applications, and Design.* 3rd Ed., USA, 2002, p. 29.

[20] A. Benaboud, A. Rufer, "A flexible, high efficiency, VSI-based HVDC transmission system with reduced harmonics," in *Proc. 2008 IEEE Power Electronics Specialists Conf.*, pp. 4117-4123.

[21] Y. Lee, A. Khaligh, A. Emadi, "Advanced integrated bidirectional AC/DC and DC/DC converter for plug-in hybrid electric vehicles," *IEEE Trans. Vehicular Technology*, vol. 58, pp. 3970-3980, Jul. 2009

[22] Z. Amjadi, and S. S. Williamson, "Power-electronics-based solutions for plug-in hybrid electric vehicle energy storage and management systems," *IEEE Trans. Industrial Electronics*, vol. 57, pp. 608-616, Feb. 2010.

[23] Y. Hu, J. Tatler, Z. Chen "A bi-directional DC/DC power electronic converter for an energy storage device in an autonomous power system," presented at the Power Electronics and Motion Control Conference, 2004.

[24] L. Fleischli, S. Lemofouet, A. Rufer, "Multichannel DC/DC converter's efficiency optimization by variable number of active channels," in *Proc. 2006 IEEE Industrial Electronics Conf.*, pp. 2581-2586.

[25] B. Destraz, Y. Louvrier, A. Rufer: "High efficient interleaved multi-channel DC/DC converter dedicated to mobile applications," in *Proc. 2006 IEEE Industry Applications Conf.*, pp. 2518-2523.

[26] R. Li, A. Pottharst, N. Frohleke, J. Bocker, "Analysis and design of improved isolated full-bridge bi-directional DC/DC converter," in *Proc. 2004 IEEE Power Electronics Specialists Conf.*, pp. 521-526.

[27] Ronald J. Parise, “Quick charge battery with internal thermal management,” in *Proc. 2000 IEEE Energy Conversion Engineering Conf.*, pp. 120-127.

[28] H. Yoo, S. Seung-Ki, Y. Park, J. Jeong, "System integration and power-flow management for a series hybrid electric vehicle using supercapacitors and batteries," *IEEE Trans. Industry Applications*, vol. 44, pp. 108-114, Jan-Feb. 2008

[29] T. Ai, T. Liang, J. Chen, “A hybrid switching method for thermal management in full-bridge inverter,” in *Proc. 2001 IEEE Power Electronics and Drive Systems Conf.*, pp. 633-637.

[30] X. Zhou, G. Wang, S. Lukic, S. Bhattacharya, and A. Huang, “Multi-function bi-directional battery charger for plug-in hybrid electric vehicle application,” in *Proc. 2009 IEEE Energy Conversion Congress and Exposition.*, pp. 3930-3936.

[31] X. Zhou, S. Lukic, S. Bhattacharya, A. Huang, “Design and control of grid-connected converter in bi-directional battery charger for plug-in hybrid electric vehicle application,” in *Proc. 2009 IEEE VPPC’09*, pp. 1716-1721.

[32] F. Koyanagi, R. Yokohama, “Monte Carlo simulation on the demand impact by quick chargers for electric vehicles,” in *Proc. 1999 IEEE Power Engineering Society Summer Meeting*, pp. 1031-1036.

[33] L. Kelly and A. Rowe, and P. Wild, “Analyzing the impacts of plug-in electric vehicles on distribution networks in British Columbia,” in *Proc. 2009 IEEE EPEC’09*, pp. 1-6.

[34] S.H. Berisha, G. Karady, R. Ahmad, R. Hobbs, and D. Karner, “Current harmonics generated by electric vehicle battery chargers,” in *Proc. 1996 IEEE International Conference on Power Electronics, Drives, and Energy Systems for Industrial Growth*, pp. 584-589.

[35] M. Basu, K. Gaughan, and E. Coyle, “Harmonic distortion caused by EV battery chargers in the distribution systems network and its remedy,” in *Proc. 2004 IEEE International Universities Power Engineering Conference (UPEC)*, pp. 869-873.

[36] J. C. Gomez and M. Morcos, “Impact of EV battery chargers on the power quality of distribution systems,” *IEEE Trans. Power Delivery*, vol. 18, pp. 975-981, Jul. 2003.

[37] O. Onar and A. Khaligh, “Grid interactions and stability analysis of distribution power network with high penetration of plug-in hybrid electric vehicles,” in *Proc. 2010 IEEE Applied Power Electronics Conference and Exposition (APEC)*, pp. 1755-1762.

[38] C. Martinez, C. Abbey, and G. Joos, “Bidirectional battery chargers for plug-in hybrid electric vehicles,” presented at the Conference on Power Systems, Winnipeg, Canada, 2008.

[39] G. Joos, M. El Chehaly, C. Martinez, “Advantages and applications of Vehicle-to-Grid mode of operation in plug-in hybrid electric vehicles,” in *Proc. 2009 IEEE EPEC’09*, pp. 1-6.

[40] C. Moreira, "MicroGrids and Electric Vehicles," in INESCPORTO Instituto de Engenharia de Sistemas E Computadores Do Porto Laboratorio Associado, Sept 18, 2009

[41] A. Giumento, A. Maitra and W. Kook, "Evaluation of PEV loading characteristics on Hydro-Québec's distribution system operations," presented at the EVS24 International Battery, Hybrid and Fuel Cell Electric Vehicle Symposium, Stavanger, Norway, 2009

[42] G. Joos, M. Dubois, "Integration of PHEVs and EVs: experience from Canada," in *Proc. 2010 IEEE Power and Energy Society General Meeting*, pp. 1-5.

[43] A. Tsang, "Identifying PEV early adopters and their needs", presented at the PHEV'09 Conference, Montreal, Canada, 2009.

[44] J. Taylor, A. Maitra, M. Alexander, D. Brooks, M. Duvall, "Evaluation of the impact of PEV loading on distribution system operations," presented at the IEEE Power Engineering Society Conference, Calgary, Canada, 2009

[45] MIT Electric Vehicle team, "A Guide to Understanding Battery Specifications," Dec 2008. [Online]. Available: http://web.mit.edu/evt/summary_battery_specifications.pdf

[46] J. Daily, K.M. Abraham, R. Plivelich, J. Landi, and M. Klein, "Electro energy bipolar wafer cell battery technology for PHEV applications," in *Proc. 2007 IEEE VPPC'07*, pp. 336-343.

[47] N.R. Pinsky, J.C. Argueta, T.J. Knipe, V.L. Grosvenor, L.A. Gaillac, M.H. Merchant, A. Cabrera, "Fast charge of lead acid batteries at the SCE EV Tech Center: battery specifications and test equipment," in *Proc. 2000 IEEE Battery Conference on Applications and Advances*, pp. 231-236.

[48] M. Dubois, "Plug-in hybrid and electric vehicles" in PHEV-Québec Test Program: A real-World test study on financial, technological and social aspects of PHEVs, Sept 28-30 2009. [Online]. Available: http://www.emc-mec.ca/phev/Presentations_en/S05/PHEV09-S05-3_MaximeDubois.pdf

[49] J. Boyes, N. Clark, "Technologies for energy storage flywheels and superconducting magnetic energy storage," in *Proc. 2000 IEEE Power Engineering Society Summer Meeting*, pp. 1548-1550.

[50] H.Y. Ayoub, D.L. Milanez, "New approaches to ideal inductors stored energy nature," in *Proc. 1998 IEEE Circuits and Systems Symposium*, pp. 199-202.

[51] Y.M Eyssa, R.W. Boom, G.E. McIntosh, and Q. Li, "A 100 kW energy storage coil for space application," *IEEE Tran. Magnetics*, vol. 19, pp. 1081-1085, May. 1983

[52] B. Johnson, J. Law, and G. Swa "Using a superconducting magnetic energy storage coil to improve efficiency of a gas turbine powered high speed rail locomotive" *IEEE Trans. Applied Superconductivity*, vol. 11, pp. 1900-1903, Mar. 2001

[53] M. Jufer, "Electric drive system for automatic guided vehicles using contact-free energy coils transmission," in *Proc. 2008 IEEE Power Electronics and Motion Control Conf.*, pp. 1-6.

[54] Mohd H. Ali, T. Murata, and T. Tamura, “A fuzzy logic-controlled Superconducting Magnetic Energy Storage (SMES) unit for augmentation of transient stability,” in *Proc. 2005 IEEE Power Electronics and Drives Systems International Conf.*, pp. 1566-1571.

[55] E. van Dijk, J.A Ferreira, P. van Gelder, “A method to charge and discharge high current energy storage coils,” in *Proc. 1999 IEEE Industry Applications Conf.*, pp. 2115-2120.

[56] J. Beno, R. Thompson, R. Hebner, “Flywheel batteries for vehicles,” in *Proc. 2002 IEEE Autonomous Underwater Vehicles*, pp. 99-101.

[57] X. FU, X. Xie, “The control strategy of flywheel battery for electric vehicles,” in *Proc. 2007 IEEE Control and Automation International Conf.*, pp. 492-496.

[58] “Investigation on Storage Technologies for Intermittent Renewable Energies: Evaluation and Recommended R&D Strategy,” Investire-Network, Contract N° ENK5-CT-2000-20336, Jun. 2003. [Online]. Available: http://www.itpower.co.uk/investire/pdfs/flywheelrep.pdf

[59] J-C. Park, G-H. Choe, “Analysis and design of PWM inverter system for flywheel energy storage system,” in *Proc. 2007 IEEE Power Electronics international Conf.*, pp. 169-173.

[60] Jack G. Bitterly, “Flywheel technology past, present, and 21st Century projections,” in *Proc. 1997 IEEE Energy Conversion Engineering Conf., pp. 2312-2315.*

[61] T. Coombs, A.M. Campbell, R. Storey, R. Weller, “Superconducting magnetic bearings for energy storage flywheels,” *IEEE Trans. Applied Superconductivity*, vol. 9, pp. 968-971, Jun. 1999.

[62] J-P. Lee, B-J. Park, Y-H. Han, S-Y. Jung, T-H. Sung, “Energy loss by drag force of superconductor flywheel energy storage system with permanent magnet rotor,” *IEEE Trans. Magnetics*, vol. 44, pp. 4397-4400, Nov. 2008.

[63] J. Zou, L. Zhang, J. Song, "Development of the 40 V hybrid super-capacitor unit," *IEEE Trans. Magnetics*, vol. 41, pp. 294-298, Jan. 2005.

[64] A. Rufer, “A supercapacitor-based energy-storage system for elevators with soft commutated interface,” *IEEE Trans. Industry Applications*, vol. 38, pp. 1151-1159, Sept-Oct. 2002.

[65] D. Iannuzzi, “Use of supercapacitors, fuel cells and electrochemical batteries for electric road vehicles: a control strategy,” in *Proc. 2007 IEEE Industrial Electronics Society Annual Conf.*, pp. 539-544.

[66] “Supercapacitors,” in Illinois Capacitors Inc [Online]. Available: http://www.illinoiscapacitor.com/uploads/papers_application/72B4ADF9DAD74E4CB7293DE6F4B62427.pdf

[67] W. L Homme, P. Delarue, P. Barrade, A. Bouscaryol, A. Rufer, “Design and control of a supercapacitor storage system for traction applications,” in *Proc. 2005 IEEE Industry Applications Conf.*, pp. 2013-2020.

[68] B. Destraz, P. Barrade, A. Rufer, “Power assistance for diesel – electric locomotives with supercapacitive energy storage,” in *Proc. 2004 IEEE Power Electronics Specialists Conf.*, pp. 677-682.

[69] A. Farkas, R. Bonert, “Ultracapacitors as sole energy storage device in hybrid electric cars ?” in *Proc. 1994 IEEE Power Electronics in Transportation*, pp. 97-101.

[70] A. Rufer, P. Barrade, D. Hotellier, S. Hauser, “Sequential supply for electrical transportation vehicles: properties of the fast energy transfer between supercapacitive tanks,” in *Proc. 2003 IEEE Industry Applications Conf.*, 1530-1537.

[71] S. Lemofouet, A. Rufer, “A hybrid energy storage system based on compressed air and supercapacitors with Maximum Efficiency Point Tracking (MEPT),” *IEEE Trans. Industrial Electronics*, vol. 53, pp. 1105-1115, Jun. 2006.

[72] S. Lemofouet, A. Rufer, “Efficiency considerations and measurements of a hybrid energy storage system based on compressed air and supercapacitors,” in *Proc. 2006 IEEE Power Electronics and Motion Control Conf.*, pp. 2077-2081.

[73] K. Morrow, D. Karner, J. Francfort, “Plug-in Hybrid Electric Vehicle Charging Infrastructure Review,” US Department of Energy, Nov. 2008. [Online]. Available: http://avt.inl.gov/pdf/phev/phevInfrastructureReport08.pdf

[74] B. Barnett, “PHEV Cost Assessment,” May. 2009. [Online] Available: http://www1.eere.energy.gov/vehiclesandfuels/pdfs/merit_review_2009/energy_storage/es_02_barnett.pdf

[75] J. Geralds, "PriusPlus History-Battery," *Plug-in Hybrid*, para. 2, Oct. 09, 2007. [Online]. Available: http://www.eaa-phev.org/wiki/Prius_PHEV_Battery_Options-CalCars

[76] P. Van den Bossche, "The electric vehicle charged by the grid: voltages and power levels,” Sept 28-30 2009. [Online]. Available:http://www.emc-mec.ca/phev/Presentations_en/S06/PHEV09-S06.4_PeterVanDerBossche.pdf

[77] “HP 602030 NCA 45 Ah/ 162 Wh Lithium Ion Cell,” Jun, 2006. [Online]. Available: http://www.gaia-akku.com/fileadmin/user_upload/downloads/cells/45AhHP_NCA.pdf

[78] M. R. Dubois, M. Desjardins, L. Tremblay, “FRESS: Fast Rate Energy Storage System”, US Patent Application 61/233,664, submitted 13 August 2009.

[79] Bo. Yang, Y. Makarov, J. Desteese, V. Viswanathan, P. Nyeng, B. McManus, and J. Pease, “On the use of energy storage technologies for regulation services in electric power systems with significant penetration of wind energy,” in *Proc. 2008 IEEE Electricity Market International Conf.*, pp. 1-6.

[80] O. Stihi, and Boon-Teck Ooi, “A single-phase controlled-current PWM rectifier” *IEEE Trans. Power Electronics*, vol. 3, pp. 453-459, Oct. 1998.

[81] S. Samineni, B.K Johnson, H.L Hess, J.D Law, “Modeling and analysis of a flywheel energy storage system with a power converter interface,” *IEEE Trans. Industry Applications*, vol. 42, pp. 42-52, Jan-Feb. 2006.

[82] VYCON, “UPS/POWER QUALITY,” *VDC Technology,* 2008. [Online]. Available: http://www.vyconenergy.com/pq/VDCtech.htm

[83] B. Vafakhah, M. Masiala, J. Salmon, A. Knight, “Emulation of flywheel energy storage system with a PMDC machine,” in *Proc. 2008 IEEE International Conference on Electrical Machines*, pp. 1-6.

[84] R. Krishnan, *Electric Motor Drives: Modeling, Analysis, and Control*. Upper Saddle River, NJ: Prentice Hall, 2001.